UK Atomic Energy Authority

UKAEA-R(15)35
November 2015

Jean-Christophe Sublet
Michael Fleming
Jiri Kopecky
Mark Gilbert
Dimitri Rochman
Arjan Koning

Summary of TENDL-2014 Verification & Validation outcomes and recommendations for future libraries

Summary of TENDL-2014 Verification & Validation outcomes and recommendations for future libraries

Jean-Christophe Sublet
Michael Fleming
Jiri Kopecky[1]
Mark Gilbert
Dimitri Rochman[2]
Arjan Koning[3]

November 2015

UK Atomic Energy Authority
Culham Science Centre, Abingdon, OX14 3DB

[1] Juko Research
Kalmanstraat 4, 1817 HX Alkmaar, The Netherlands
[2] Paul Scherrer Institut
OHSA/D05, Ch-5232 Villigen PSI, Switzerland
[3] IAEA Nuclear Data Section
Vienna International Centre, A-1400 Vienna, Austria

Contacts Dr Jean-Christophe Sublet
Dr Michael Fleming

UK Atomic Energy Authority
Culham Science Centre, Abingdon, OX14 3DB,
UK

Telephone: +44 (0)1235-466400
email: jean-christophe.sublet@ccfe.ac.uk

Telephone: +44 (0)1235-466884
email: michael.fleming@ccfe.ac.uk

Facsimile: +44 (0)1235-463435

Website: **http://www.ccfe.ac.uk/fispact.aspx**

Disclaimer

Neither the authors nor the United Kingdom Atomic Energy Authority accept responsibility for consequences arising from any errors either in the present documentation or the FISPACT-II code, or for reliance upon the information contained in the data or its completeness or accuracy.

CCFE is the fusion research arm of the United Kingdom Atomic Energy Authority.

CCFE is certified to ISO 9001 and ISO 14001.

Acknowledgement

To all the experimentalists since the dawn of the nuclear age who have contributed to the databases that we take for granted.

Executive Summary

The TALYS-generated Evaluated Nuclear Data Libraries (TENDL) are truly general-purpose nuclear data libraries assembled from the outputs of the T6 nuclear model codes system for direct use in both basic physics and engineering applications. The most recent TENDL-2014 version is based on both default and adjusted parameters of the most recent TALYS, TAFIS, TANES, TARES, TEFAL, TASMAN codes wrapped into a Total Monte Carlo loop for uncertainty quantification. TENDL-2014 contains complete neutron-incident evaluations for all target nuclides with Z $<$ 116 (Livermorium) with half-life longer than 1 second (2632 isotopes), up to 200 MeV, with covariances and all reaction daughter products including isomers of half-life greater than 0.1 second. With the added High Fidelity Resonance (HFR) approach, all resonances are unique, following statistical rules.

The validation of the TENDL-2014 neutron-induced library against standard, evaluated, microscopic and integral cross sections has been performed against a newly compiled UKAEA database of thermal, resonance integral, Maxwellian averages, 14 MeV and various accelerator-driven neutron source spectra. This has been assembled using the most up-to-date, internationally-recognised data sources including the Atlas of Resonances, CRC, evaluated EXFOR, activation databases, fusion, fission and astrophysics experiments. Excellent agreement with TENDL-2014 values is found with a small set of errors within the reference databases and TENDL-2014 predictions.

This report is a compendium of the discrepancies found in the set of UKAEA validation efforts. These should be re-examined and, where appropriate, lead to re-evaluations for future TENDL distributions. These can be generally broken down as: (1) updating input parameter databases, (2) modification of resolved resonance formalism, (3) improving the automated use of CALENDF to generate statistically resolved/extended resonance regions and (4) re-examination of pre-equilibrium mechanisms for specific channels/energies.

Contents

1 Overview

The documents from which this report draws from span more than a thousand pages with thousands of figures and tables. From a huge database, the *vast* majority shows excellent agreement between TENDL-2014 predictions and experimental data taken from a wide range of measurement techniques. Those considered within the verification and validation reports are:

CCFE-R(15)25 [1] Fusion decay heat measurements from JAEA FNS – data summarised within CCFE-R(15)27 but detailed data complements analysis

CCFE-R(15)27 [2] Integral cross section measurements from D-T fusion and accelerator systems juxtaposed with all EXFOR differential data on the channel

UKAEA-R(15)29 [3] Integral astrophysical cross sections from Maxwellian spectra with kT=1 to 100 keV

UKAEA-R(15)30 [4] Thermal cross sections as differential or Maxwellian averages and resonance integrals

From the studies in the above reports, a set of discrepancies has been compiled for easy reference. These are broken down into thermal, integral resonance, average astrophysical Maxwellian and accelerator-source data. Following this are a few other observations which highlight issues with the way TENDL libraries are formed, including some format errors and coding bugs within T6.

Note that several nuclides appear in multiple sections/tables, largely due to the fact that incorrect parameters in one regime will affect others, *i.e.* thermal inaccuracies affect resonance integrals and misallocated resonances affect wide-spectrum integral measurements in general. Each and every measurement should be considered in evaluation, as demonstrated by the examples in Section 2.

1.1 Thermal cross sections

The discrepancies in thermal cross sections are easily remedied with modification of input databases. The 69 reaction channels which show disagreement of C/E <0.5 or >2.0, using the newly compiled UKAEA database, are summarised in Table 1. The 20 which differ by a factor of ten or more are highlighted, with six clearly due to mb $\leftrightarrow$ b errors.

Note that the majority of the channels with discrepancies are the partial, isomeric production reactions. This is primarily due to the way TENDL-2014's unique `MF=9` files are generated, which does not rely upon the reference values included in the UKAEA database. It is still impressive that TENDL-2014 typically predicts accurate isomeric production, but future libraries should take advantage of this additional information.

1.2 Resonance integrals

While thermal cross sections may be modified with one input parameter, integral measurements over resonance regions or with complex spectra spanning the majority of the resolved resonance range are less easily translated into model and/or parameter adjustments. The 97 reaction channels which show disagreement with C/E <0.5 or >2.0, using the newly compiled UKAEA database, are summarised in Table 2. Of those 97 channels, 24 differ by a factor of ten or more and are highlighted.

1.3 Astrophysical MACS

For astrophysical MACS, most of those listed below have either ENDF/B-VII.1 or JENDL-4.0 files containing MF=2 resonance data that better reproduce the experimental values. Those listed in red are the product of statistical model calculations as published in the KADoNiS database:

JENDL-4.0: ^{58}**Ni,** ^{65}**Zn,** ^{70}**Ge,** ^{76}**Se,** ^{82}**Se,** ^{84}**Sr,** ^{104}**Ru,** ^{112,114,118}**Sn,** ^{123,124,128}**Te,** ^{140}**Ce,** ^{146}**Nd,** ^{144,153}**Sm,** ^{160}**Tb,** ^{186}**Os,** ^{198,200,202,204}**Hg,** ^{204,207,208}**Pb**

ENDF/B-VII.1: ^{69,71}**Ga,** ^{103}**Rh,** ^{156,158}**Dy,** ^{205}**Tl**

A small set of capture reactions have very large discrepancies due to some erroneous input parameters, which are summarised in Table 3, alongside the ENDF/B-VII.1 and JENDL-4.0 values. Note that only three broad energies are selected and the comparisons are not meant as a proposal to draw data from a different library. Of the nuclides identified in this table, the ^{3}He comes directly from ENDF/B-VII.1 but the remaining are generated by T6. While the low-Z carbon and oxygen files pose their own, specific modelling issues, the remaining should be directly addressable. Note that the ^{200}Hg has discrepant thermal and resonance integral values as well, but has very good agreement with the other libraries.

One nuclide, ^{186}Os, experienced a bug in evaluation which resulted in **no resolved resonances** being included in the MF=2 file, except those statistically resolved using CALENDF.

These temperature-dependent average cross sections must be explored in more detail than can be provided by one number. In a subsequent section individual channel analysis will be presented as an example.

1.4 Other integral cross sections

The integral values summarised in CCFE-R(15)27 are drawn from numerous experiments with substantially different neutron spectra. These include deuteron beams of a variety of energies/currents incident on beryllium, lithium and tritiated targets, as well as spontaneous californium measurements. The spectral qualification varies tremendously from the spontaneous spectrum to what are effectively MCNP simulations 'unfolded' using a handful of activation foil measurements and, for one dataset, theoretical analytic spectra. Some measurements are of direct gamma lines of product nuclides, while some use

spectroscopic or total decay heat and isolate cooling times where one nuclide is strongly dominant.

Great care must be exercised when considering these integral measurements and this is why differential EXFOR values are juxtaposed with the microscopic cross section for each channel in that report. Disagreement with integral values is often insufficient to draw any conclusions without some corroborating information. As a result, the list of reactions which should be re-evaluated based on those results is *not* a list of channels with some threshold C/E, but a carefully selected list based on the judgement of those authors is presented in Table 4. For the comparison with FNS decay heat measurements, further information is provided by CCFE-R(15)25, which probes the detailed decay heat of each sample.

^{92}Mo(n,p): Isomeric branching errors in `MF=9` result in sum of partials greater than total

^{115}In(n,g): Isomeric branching errors in `MF=9` result in sum of partials greater than total

^{177}Hf(n,n')^{177n}Hf: Isomeric product missing from file while measurements exist

^{181}Ta(n,t)^{179n}Hf: Isomeric product missing from file while measurements exist

^{182}W(n,a)^{179n}Hf: Same isomeric product as above *exists* in file but over-predicted against both differential and integral values

1.5 Other format or numerical irregularities

A few other errors in the TENDL file construction have been found which point to coding issues which must be addressed in future T6 versions. These can be summarised as:

(1) Some 'experimental' values need to be re-examined and potentially removed from databases used in the generation of files, such as the spurious thermal ^{55}Fe (n,α) at 170 b (instead of 27 mb [5]) which appeared in previous TALYS databases[1]

(2) Inelastic channels must ensure that thresholds are respected in partial level production – `MF=3` and `MF=10` values should match (found by [6])

(3) Inelastic production channels must be examined for irregularities due to file 'splicing'

(4) Remainder partial yields must have methods for accommodating new channels without producing illogical features in existing reaction channels

Examples of those points above are shown in **(1)** Figure 1 **(2)** Figure 2 **(3)** Figure 3 **(4)** Figures 4 and 5.

[1] *nb* This correction was made in TENDL-2013 but has crept back into the 2014 version.

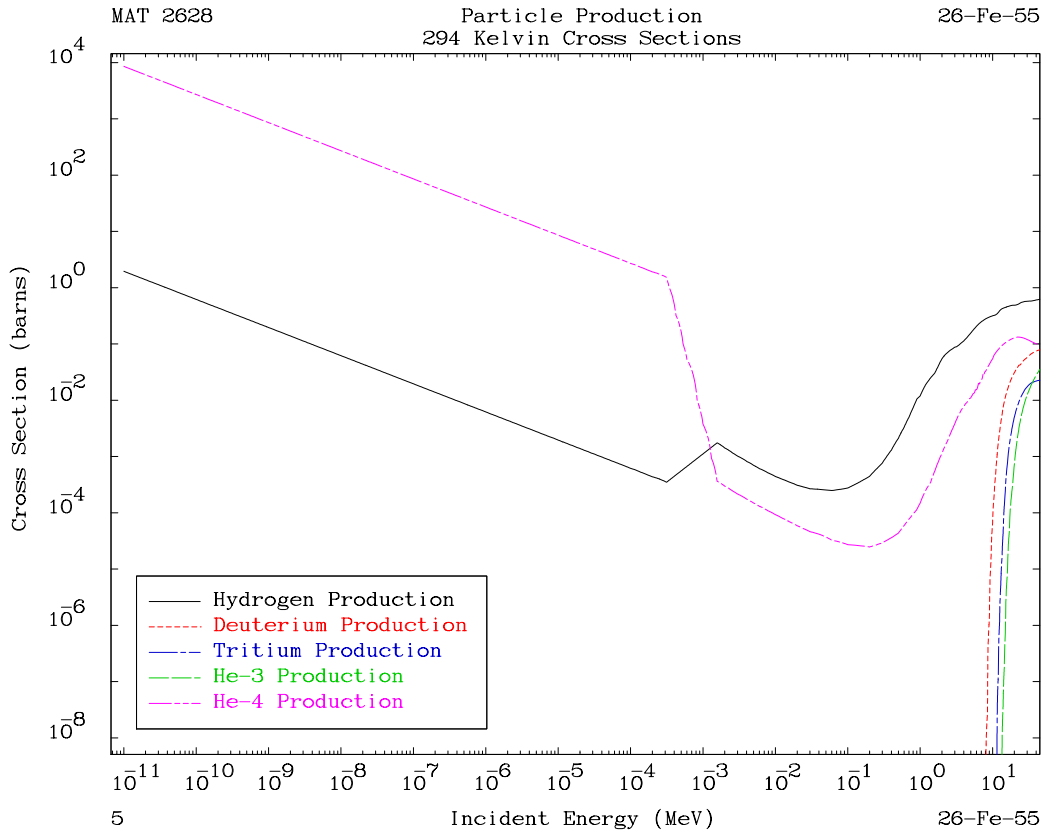

Figure 1: TENDL-2014 microscopic ^{55}Fe (n,α) cross sectionn against other particle production channels.

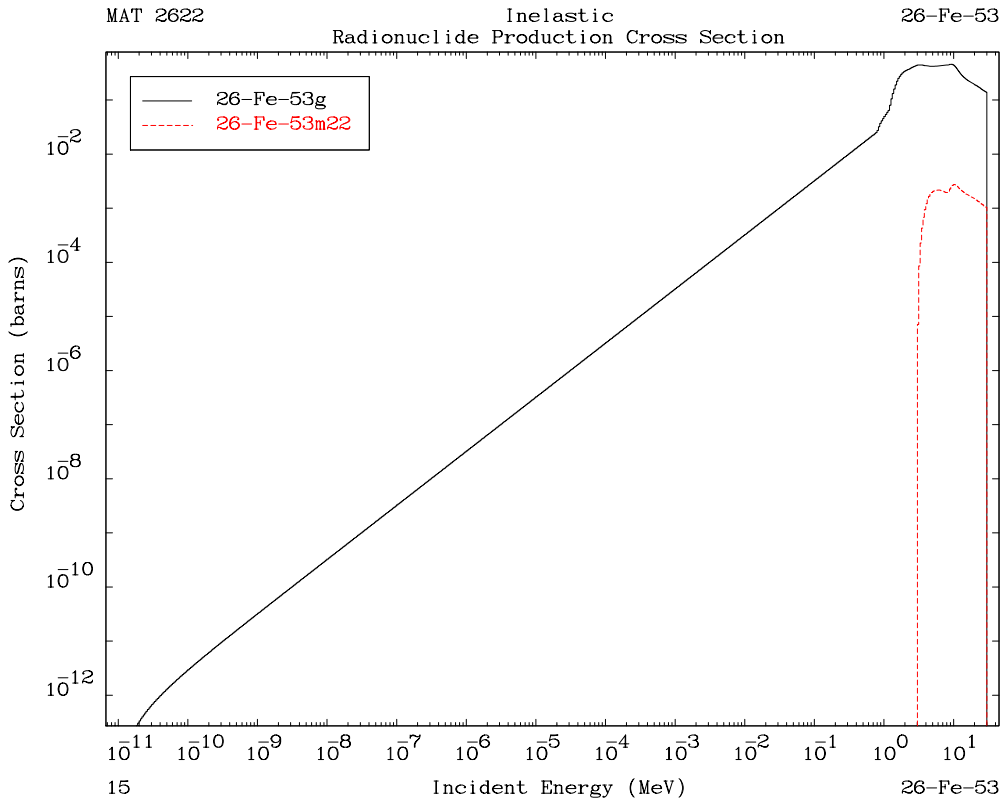

Figure 2: TENDL-2014 microscopic ^{53}Fe (n,n') inelastic cross sections for the ground and first isomer production.

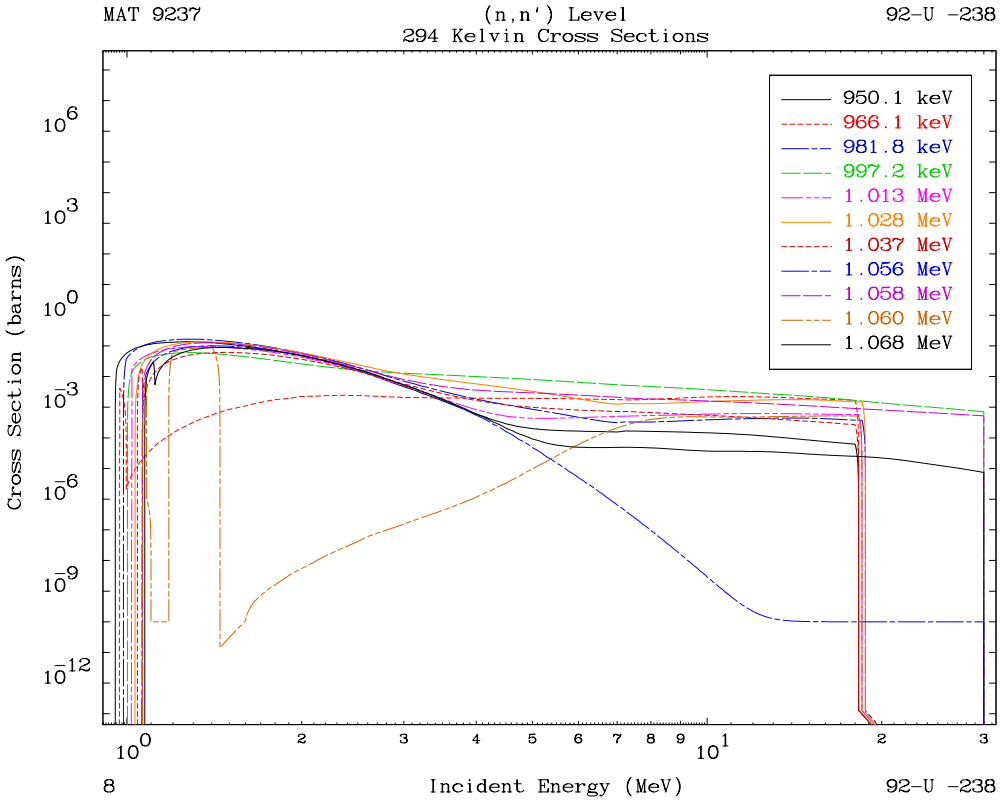

Figure 3: TENDL-2014 microscopic ^{238}U (n,n') inelastic cross sections for the first 11 levels.

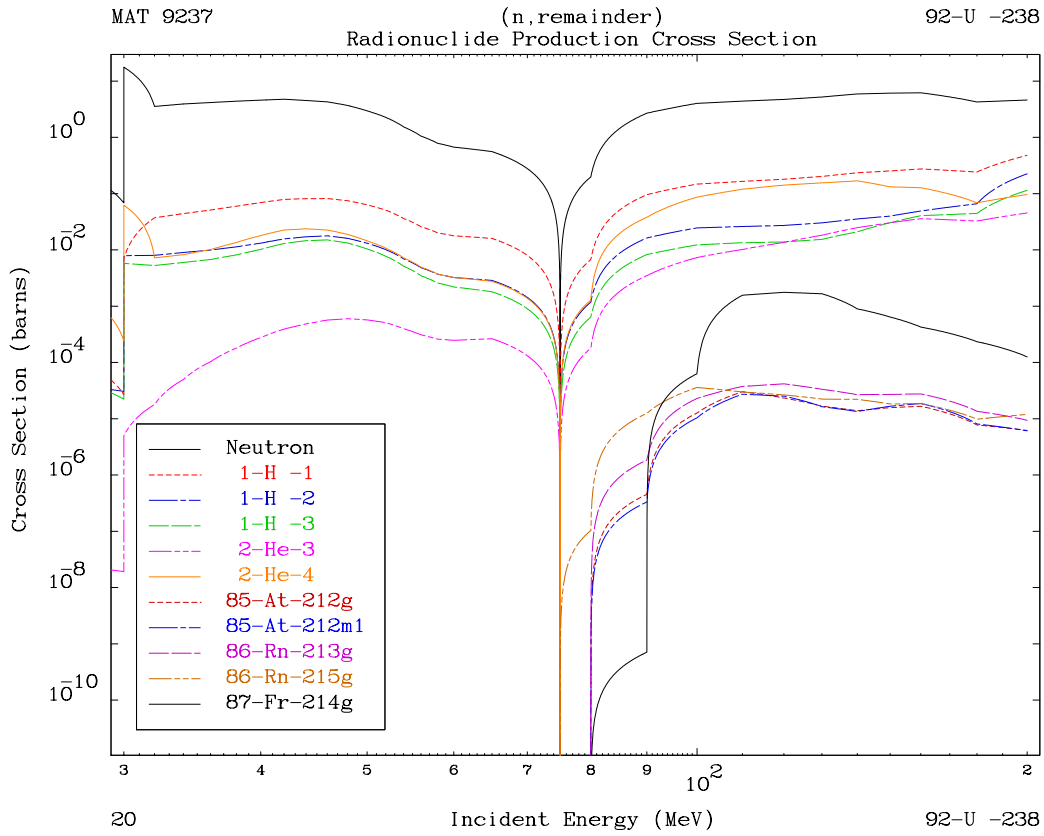

Figure 4: TENDL-2014 microscopic ^{238}U (n,remainder) production cross sections.

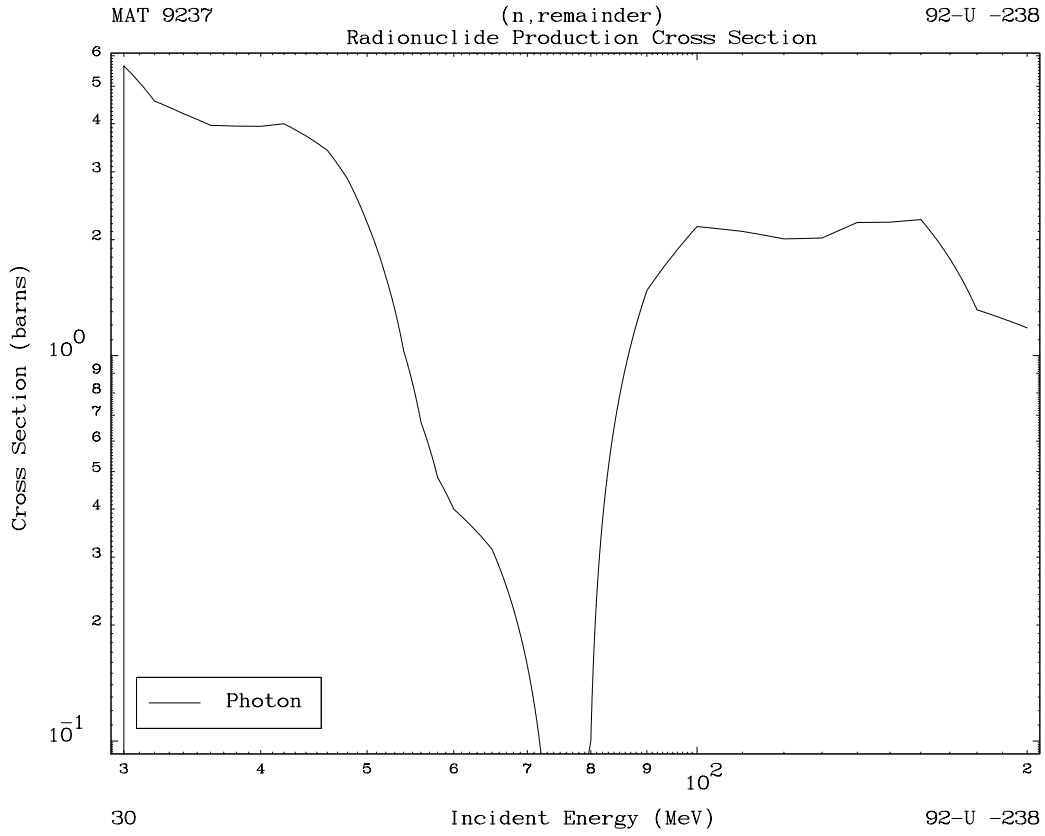

Figure 5: TENDL-2014 microscopic ^{238}U (n,remainder) photon production cross section.

2 Individual channel analyses

The integral measurements used in the cited validation reports possess a wealth of information which can inform future TENDL evaluations. While the list of discrepancies highlights those nuclides which should be considered for re-evaluation, this section provides some insights into the types of analyses that are possible with the integral data.

Three subsections are provided: (1) a clear example with discrepant decay heat measurements and differential disagreements (2) a more subtle example with multiple integral measurements conflicting with some differential data and (3) a set of five (statistically and experimentally) resolved resonance examples where TENDL-2014 resonance parameters should be re-evaluated – through a combination of formalism changes and alteration to how TARES employs CALENDF.

2.1 Example: ^{181}Ta(n,γ)

CCFE-R(15)25 and 27 consider integral values with neutron spectra ranging from thermal energies up to 14, 20, and above 50 MeV, largely explored for D-T fusion reactor applications and the accelerator systems that are proposed for materials studies. The decay heat measurements from the JAEA FNS facility [7, 8] were analysed in CCFE-R(15)25 using TENDL-2014, ENDF/B-VII.1, JENDL-4.0 and JEFF-3.2 neutron-induced libraries. While the report generally found significantly better agreement for TENDL-2014 simulations (largely due to complete isomeric production channels – although a few *total* channels are missing in the others), calculations for several materials showed large differences. For example, consider the seven hour irradiation of tantalum at FNS as summarised in Figure 6. While the prediction for ^{180}Ta production agrees with the FNS results, the heat between 10-400 days are under-predicted due to some combination of ^{181}Hf and/or ^{182}Ta cross sections. While the first of these measurements are due to a clear mixture of both nuclides, after 100 days the ^{181}Hf contribution drops off and the final two measurements are 90%+ ^{182}Ta. The only reaction channel for this nuclide is the ^{181}Ta(n,γ), which only has short-lived or low-yield isomers.

The ^{181}Ta(n,γ)^{182}Ta reaction was also measured in a campaign at the ENEA Fusion Neutron Generator (FNG) [9], which also indicated an under-prediction of ^{182}Ta production with a similar experimental result. To probe the cross sections in more detail, Figure 7 shows the microscopic cross section along with EXFOR data, the FNS 7 hour irradiation neutron spectrum and the collapsed, microscopic reaction rate. The large drop in microscopic cross section at 4-20 MeV does not appear to agree with the experimental data, of which both total and partial measurements show significant disagreement with the TENDL-2014 predictions – even the n-isomer production measurements are 1-2 orders of magnitude greater than the TENDL-2014 total.

This channel is one of the few cases where normalisation to a standard file has been used to override the TALYS predictions – in this case using IRDFF [10]. Upon closer inspection, the IRDFF ^{181}Ta(n,γ) data is taken from JENDL/D-99[2]. The ENDF/B-VII.1 `MF=1` comments are more straightforward:

[2]Although as is apparently standard practice, IRDFF-1.05 references IRDFF-2002, which references JENDL-3.3, which indirectly references the `casthy` evaluation used for JENDL/D-99. For the sake of reproducibility and traceability, more direct citation should be encouraged.

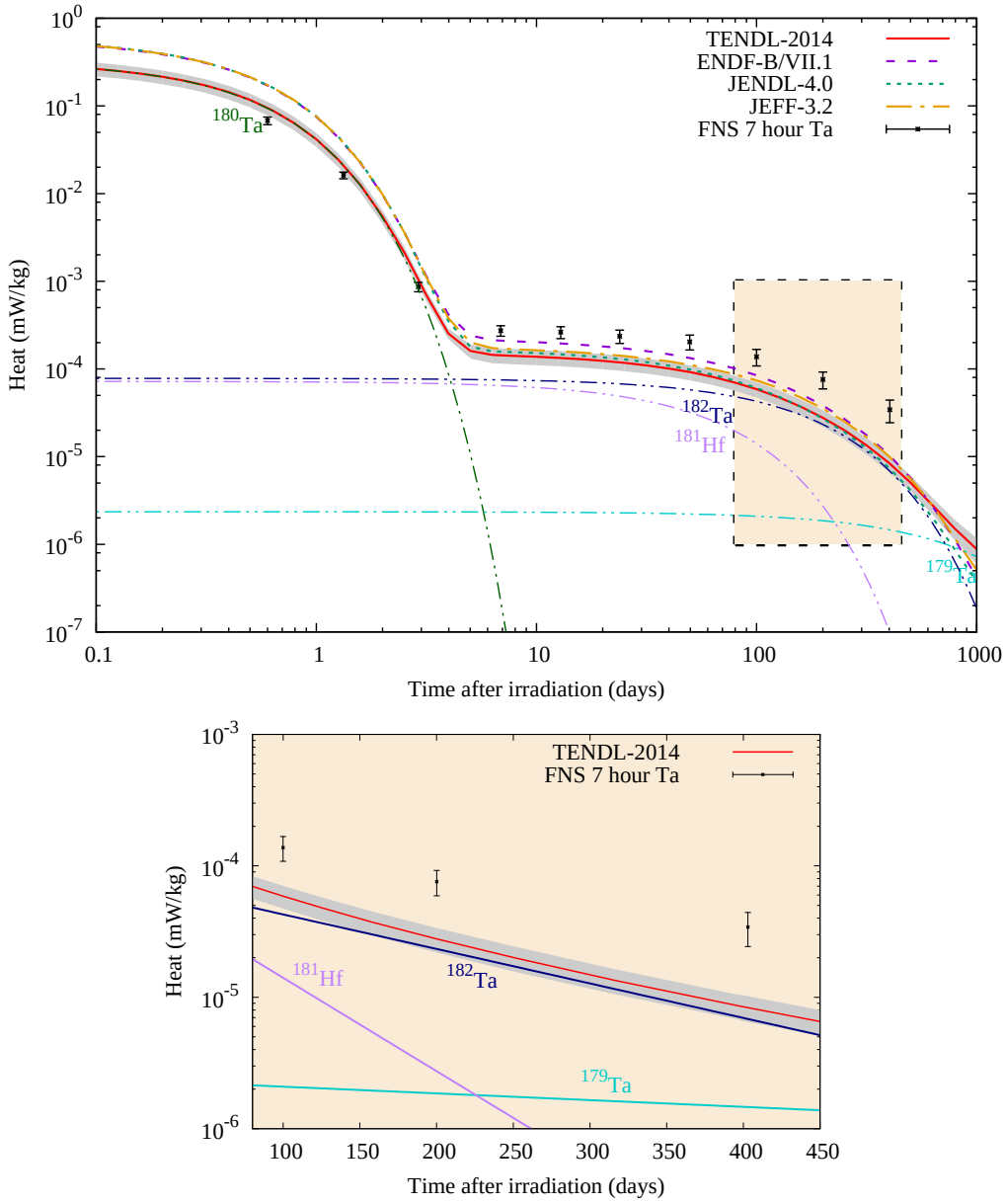

Figure 6: Decay heat simulations using TENDL-2014 and other libraries against the FNS 7 hour tantalum irradiation results. Partial heat curves for individual product nuclides are identified for the TENDL-2014 simulation.

```
 73-Ta-181 LLNL       EVAL-Jan11 I.J. Thompson and N.C. Summers   7328 1451     5
           DIST-      REV-                              20111222   7328 1451     6
----ENDF/B-VII.1      MATERIAL 7328                                7328 1451     7
-----INCIDENT NEUTRON DATA                                         7328 1451     8
------ENDF-6 FORMAT                                               7328 1451     9
                   ENDL File Documentation                         7328 1451    10
 ============================================================      7328 1451    11
Fixed QM in MF3/MT91 and ZA floating point in MF6                  7328 1451    12
Fixed resonance background                                         7328 1451    13
ENDL-2009                                                          7328 1451    14
     Neutron transport library made by Talys                       7328 1451    15
          with global nuclear models                               7328 1451    16
```

```
                                                                  7328 1451   17
Customisation: I.J. Thompson, N.C. Summers, D. Brown,             7328 1451   18
               Lawrence Livermore National Laboratory, USA        7328 1451   19
Code Authors: A.J. Koning and D. Rochman,                         7328 1451   20
              NRG Petten, The Netherlands                         7328 1451   21
Original Code Description: A.J. Koning and D. Rochman,            7328 1451   22
                           NRG Petten, The Netherlands            7328 1451   23
                                                                  7328 1451   24
************** G E N E R A L   I N F O R M A T I O N ************ 7328 1451   25
                                                                  7328 1451   26
This evaluated data file is based primarily on the nuclear model  7328 1451   27
code Talys [kon07], version 1.0.                                  7328 1451   28
It is part of a large collection of isotopic                      7328 1451   29
evaluations, all created by running Talys with default input      7328 1451   30
parameters.                                                       7328 1451   31
```

The ENDF/B-VII.1 which appeared to be similar to TENDL-2014 is in fact a TALYS-evaluated nuclear data file, made before the TALYS authors produced nuclear data libraries themselves. TALYS-1.0 was released in 2007 and the current TALYS-1.7 represents some eight years of model improvements, re-evaluation of input parameters, module additions, bug-fixes, and other code development[3]. All TALYS-based predictions give superior agreement with both the differential and integral values, while also making an important point about IRDFF: dosimetry files are only as good as their validation, which typically does not cover any whole file. This capture reaction underlines this point, where the 5+ MeV cross section was never validated and is completely specious.

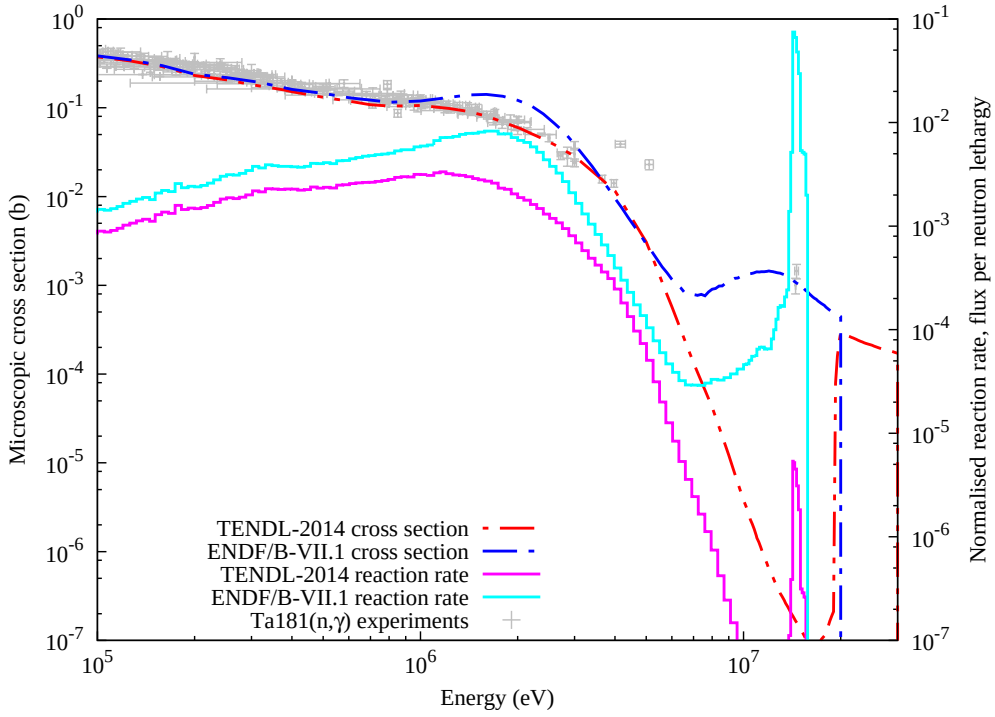

Figure 7: Microscopic cross section for ^{181}Ta(n,γ) with differential EXFOR measurements, the FNS neutron spectrum and corresponding reaction rate as calculated by FISPACT-II. Note the large drop from 4-20 MeV which disagrees with experiment.

[3]See, for example, Sections 1.1-1.4 and Appendices A-C of the TALYS 1.7 manual [11]

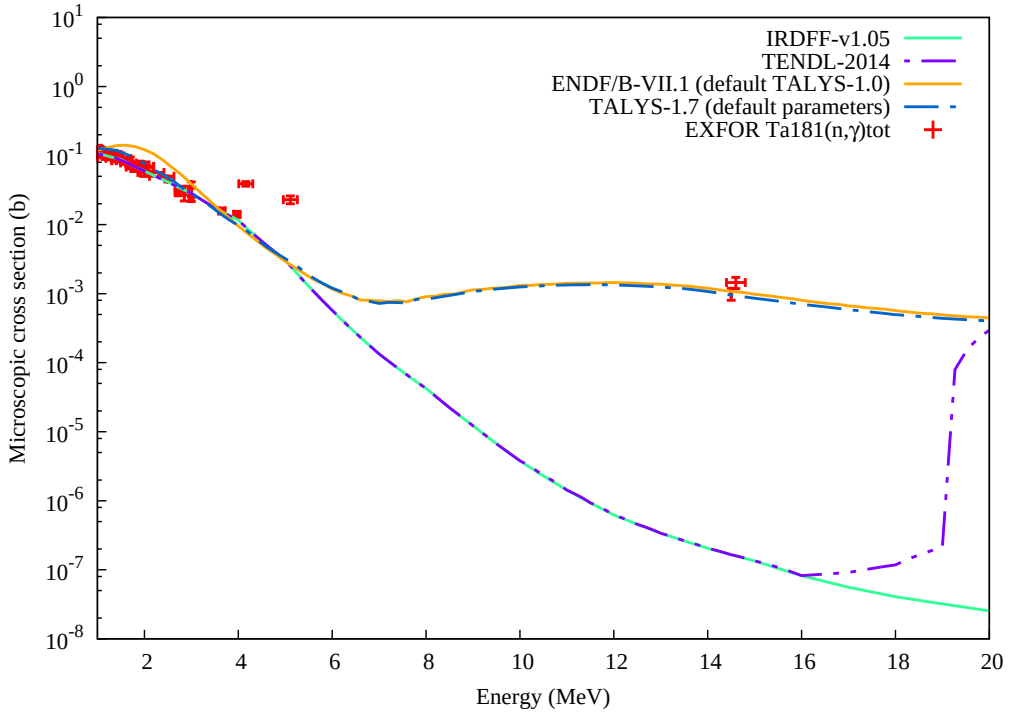

Figure 8: Microscopic cross section for ^{181}Ta(n,γ) with differential EXFOR measurements. IRDFF-v1.05 clearly under-estimates at 14 MeV, while all TALYS calculations produce reasonable agreement, including the TALYS-generated ENDF/B-VII.1.

2.2 Example: ^{180}Hf(n,p)

While integral measurements (from decay heat or other methods) cannot provide a detailed picture of microscopic cross sections, they are helpful for identifying areas for improvement in the microscopic data. Multiple integral measurements with either complementary spectra or different measurement techniques can provide more information. Two separate D-T neutron sources, the JAEA FNS and ENEA FNG, were used for total decay heat and spectroscopic decay heat measurement campaigns [7, 12, 13].

While the neutron spectra for each is quite similar and the irradiation durations are identical, the combination of measurements gives a more robust picture, as shown in Figure 9. *Note* that flux and spectral differences result in different nominal values – the FNG results and simulations have been renormalised to plot alongside the FNS results.

For the FNS data, ^{179m}Hf is 95%+ dominant for the first measurements and, within errors/uncertainties, TENDL-2014 gives reasonable agreement between simulation and experiment. In the subsequent measurements ^{180}Lu is 70%+ dominant and, although the TENDL nuclear data uncertainty for the responsible reaction channel is quite large ($\pm$56%), the simulated heat is still outside the uncertainty band. The second dominant nuclide during 4-15 minutes cooling time, ^{180m}Hf, becomes strongly dominant in the last measurements and is clearly over-predicted (providing another of the discrepancies in Table 4) – suggesting that the ^{180}Lu under-prediction is actually even more significant.

^{180}Lu radiates the majority of its decay energy through γ radiation, while ^{178}Lu decay energy is almost exclusively emitted through β-decay. The small number of FNG mea-

surements only cover the region of ^{180}Lu dominance and supports the claim that the TENDL-2014 ^{180}Hf(n,p)^{180}Lu cross section is too low. Just as with the FNS data, the greatest differences occur when ^{180}Lu is the most dominant heat contributor, around 5-6 minutes cooling.

Two sets of differential measurements were made using OKTAVIAN and the same FNS facility [14, 15]. These are plotted in Figure 10 against the microscopic TENDL-2014 cross section, the FNS position 3 flux for the decay heat measurement and the collapsed, energy-dependent reaction rate. The uncertainty band is the TENDL-2014 variance, while the uncertainty in Figure 9 represents the full, collapsed covariance. 99% of the reaction rate occurs between 14.2 and 15.8 MeV. While the differential measurements appear to agree with each other and the TENDL-2014 cross section curve, that two integral measurements (including one of the same facilities) give discrepant measurements warrants some additional analysis of this channel.

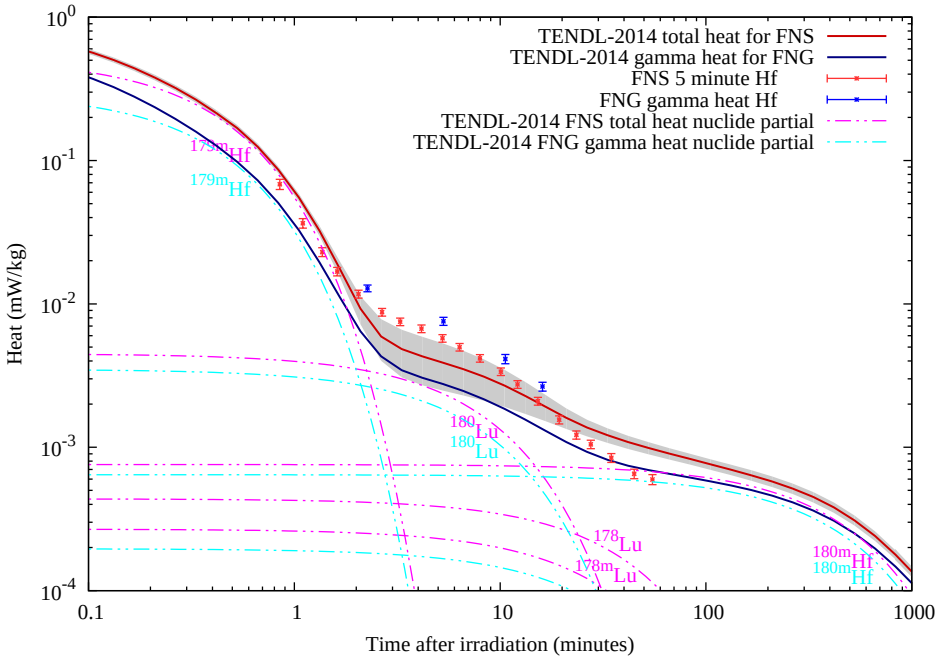

Figure 9: Decay heat simulations using TENDL-2014 and other libraries against FNS and FNG 5 minute hafnium irradiation results. Partial heat curves for individual product nuclides are identified for the TENDL-2014 simulation. Note that the FNG values are partial gamma heat and have all been renormalised to plot against the FNS data.

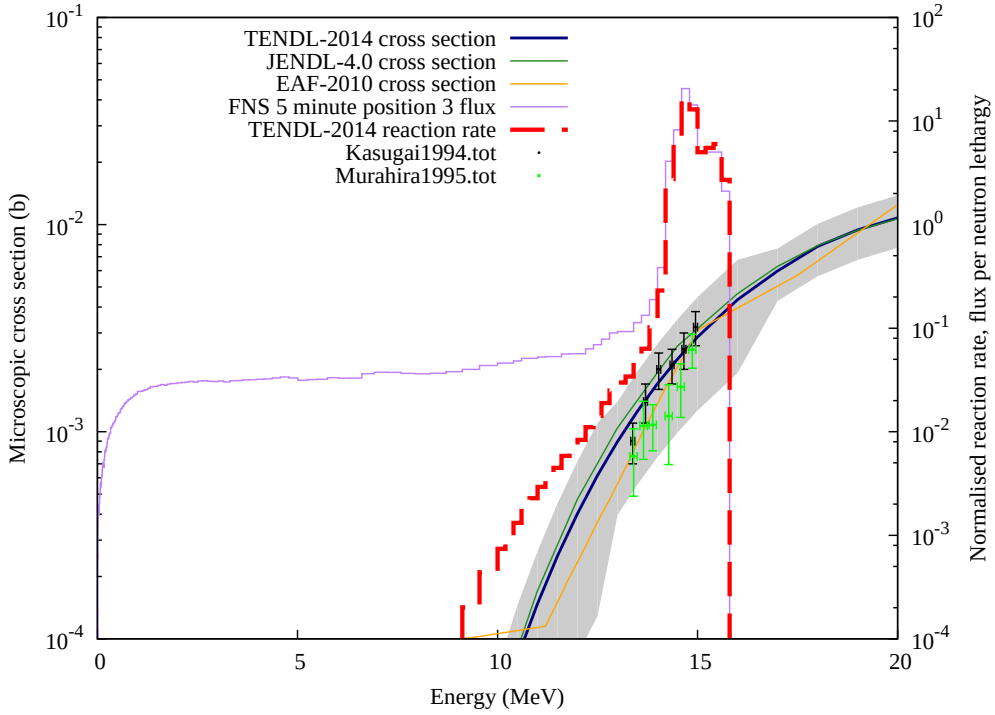

Figure 10: Microscopic cross section for ^{180}Hf(n,p) with differential EXFOR measurements, the FNS neutron spectrum and corresponding reaction rate as calculated by FISPACT-II.

2.3 Examples: Resonance parameters and (n,γ) reactions

The resolved resonance region is a complex component for nuclear data, where a large set of resolved resonance parameters are used to reconstruct the cross section. While ToF measurements can probe detailed structures over a wide energy range, nuclides with these measurements are few and far between – and most nuclides will never be studied at that level. Integral Maxwellian measurements exist for many nuclides without more detailed study, which affords some opportunity for validation. To determine what incident neutron energies are being probed by the MACS, a Doppler-broadened cross section collapsed with a Maxwellian spectrum gives the energy-dependent reaction rate. Three different types of improvements can be discerned from the examples that follow:

(1) In some cases `LRF` selection and/or choices for negative resonances must be performed more intelligently to acquire low-energy resonances which agree with experiment

(2) High-fidelity resonances which are added to nuclides with *no resolved parameters* must be mindful of experimental data

(3) High-fidelity resonance extensions to resolved resonance regions must be re-evaluated for some nuclides, where average parameters are not being faithfully reproduced

The ^{34}S an^{28}Si examples below show cases of **(1)**, where the $1/v$ below the first resonance and shape of the first resonance are modified by formalism and negative resonances. The ^{34}S example is quite straight-forward, since the region immediately before the first

resonance is precisely that of stellar plasma energies. The ^{28}Si is more subtle and includes multiple apparent contradictions within the EXFOR data. What is clear is that the first resonance plays the central role in the reaction rates over all temperatures with kT>10 keV, which results in a substantial over-prediction. The increased first resonance integral with the TENDL-2014 description produces a more pronounced over-prediction.

The following ^{46}Ca and ^{65}Zn examples show two set of statistically resolved resonance ranges which conflict with experimental data. The ^{64}Ca case involves a first giant resonance which dominates the reaction rates below kT=50 keV and gives a substantial over-prediction. The following compensation to match the resonance integral then results in a higher-temperature under-prediction. The ^{65}Zn capture MACS are very well predicted by the ENDF/B-VII.1 file, which includes a simple $1/v$ cross section over virtually all of the astrophysical reaction energies. While the statistically resolved resonances in TENDL-2014 do not affect the agreement with an apparent 'differential' measurement by Bao, this is in fact a Maxwellian which covers the newly-introduced resonances – resulting in non-trivial disagreement.

The ^{144}Sm is an example of the statistically extended resolved resonance region which does not respect the average values which have been experimentally determined. Moreover, they likely do not reproduce the average values which would be generated from standard statistical treatment of the unresolved resonance region. The result is an obviously under-predicted cross section through this region which dips the otherwise good agreement with KADoNiS.

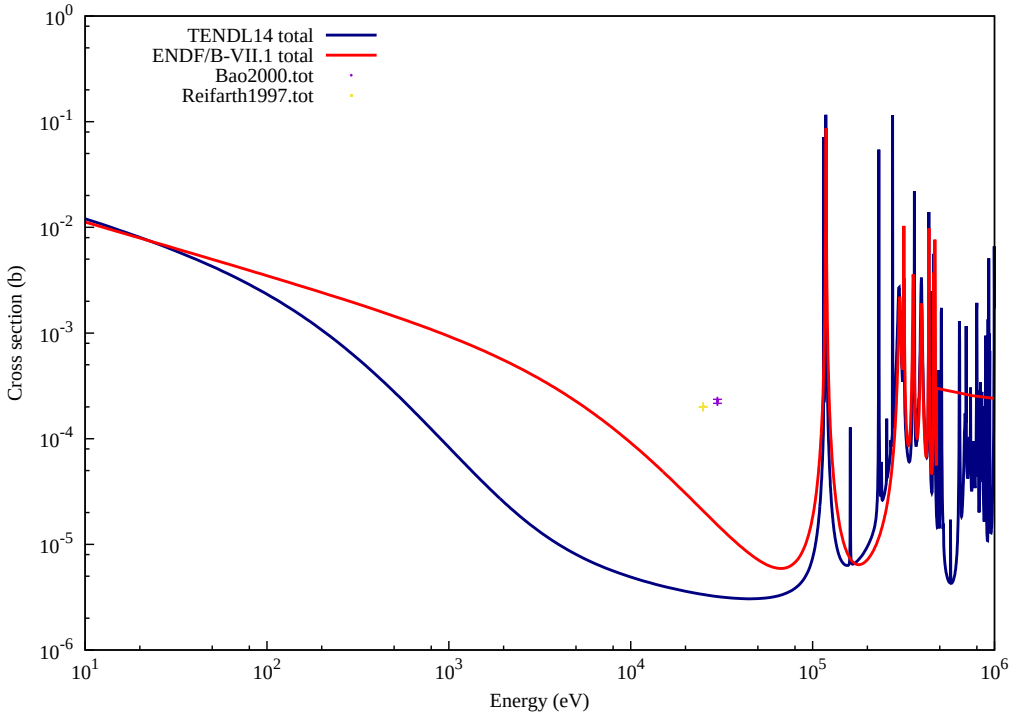

Figure 11: Microscopic ^{34}S capture cross sections with EXFOR datapoints. Differences in formalism and negative resonances dramatically alter the pre-first resonance cross section.

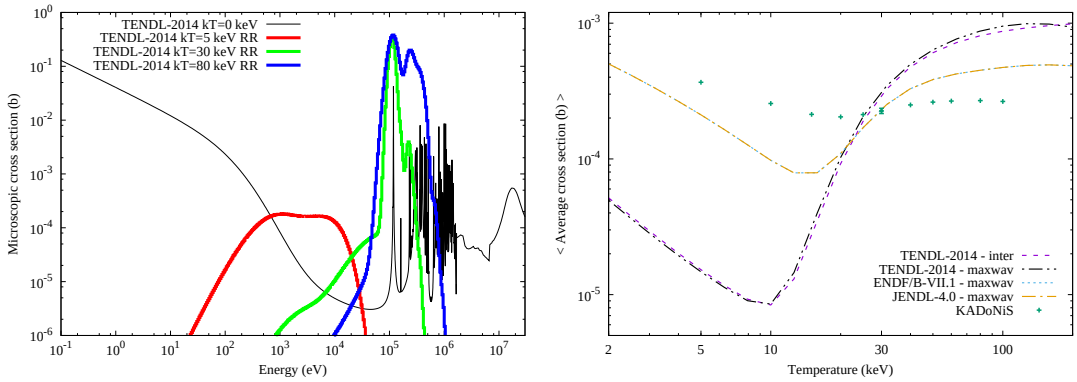

Figure 12: Microscopic kT=0 ^{34}S capture cross sections with normalised reaction rates for kT=5, 30 and 80 keV (left). Comparison of average Maxwellian capture cross section over temperature for ^{34}S (right). Since the energy region below 100 keV is affected by the `MF=2` differences and is responsible for the vast majority of the sub-30 keV reaction rate, it produces a large discrepancy with the experimental data.

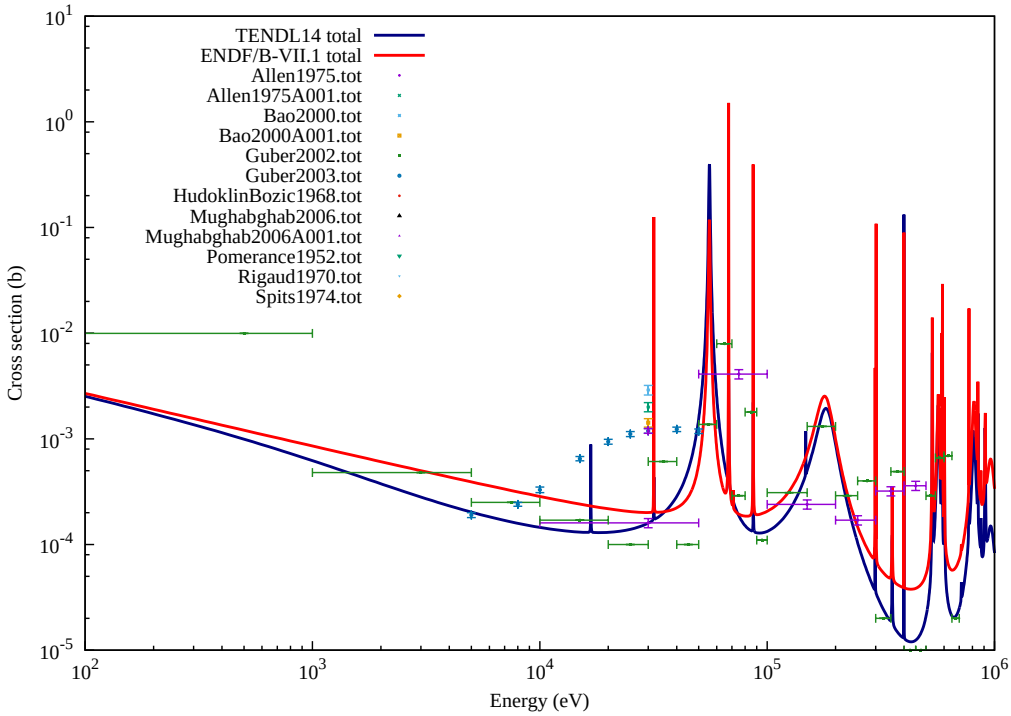

Figure 13: Microscopic ^{28}Si capture cross sections with EXFOR datapoints. A difference in formalism and negative resonances results in a significant difference in the $1/v$ contour before the first major resonance, which also has a substantially different shape and much greater total integral.

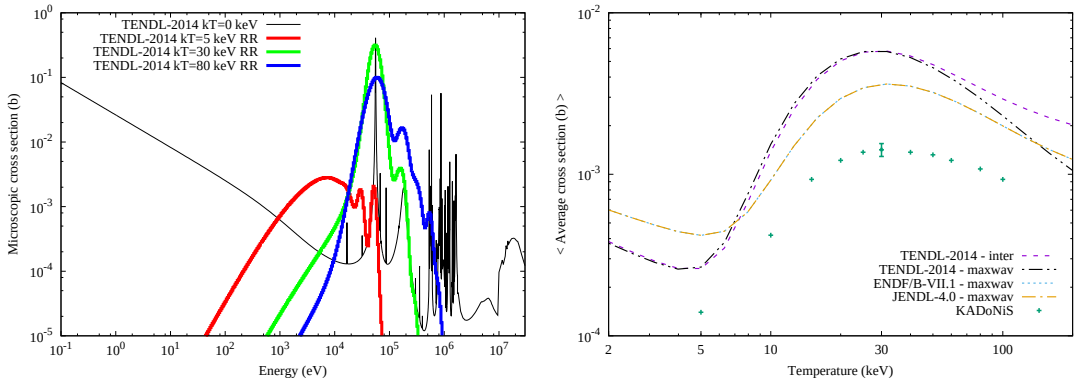

Figure 14: Microscopic kT=0 ^{28}Si capture cross sections with normalised reaction rates for kT=5, 30 and 80 keV (left). Comparison of average Maxwellian capture cross section over temperature for ^{28}Si (right). The over-prediction in the first resonance is largely responsible for the large over-prediction at all temperatures, while some systematic over-prediction is likely at fault for lower temperatures.

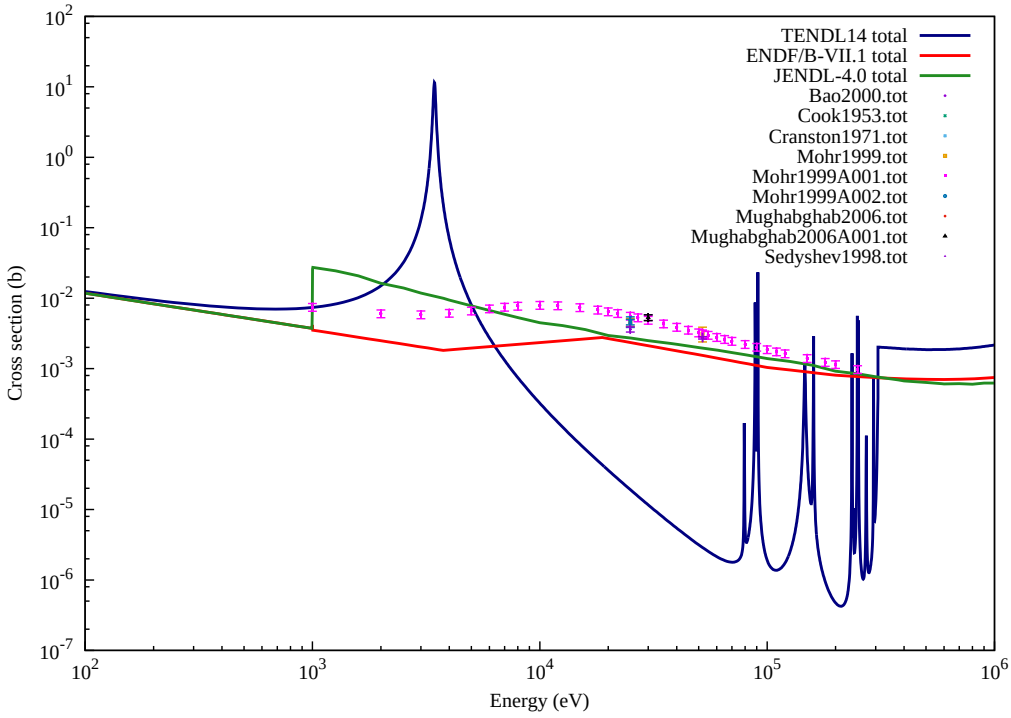

Figure 15: Microscopic ^{46}Ca capture cross sections with EXFOR datapoints. The statistically resolved resonances introduce structure which does not match with the experimental data.

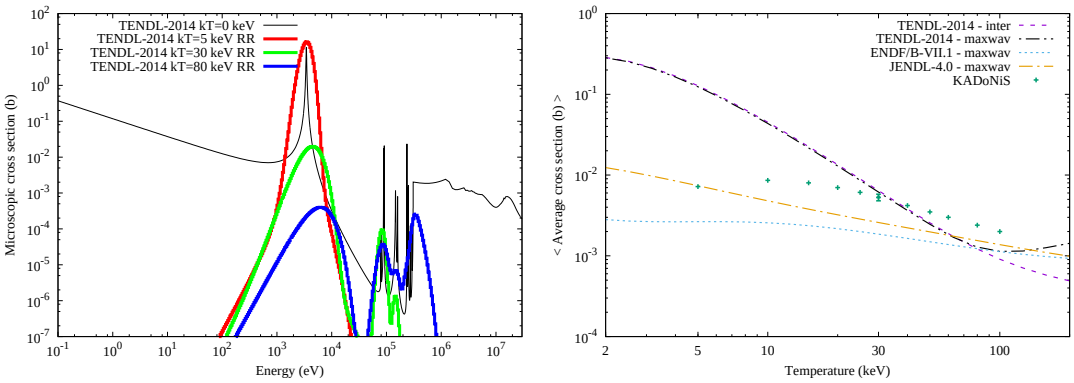

Figure 16: Microscopic kT=0 ^{46}Ca capture cross sections with normalised reaction rates for kT=5, 30 and 80 keV (left). Comparison of average Maxwellian capture cross section over temperature for ^{46}Ca (right). The first resonance dominates the reaction rate for all temperatures below kT=50 keV and produces the over-preciction, while at higher temperatures the normalisation to a resonance integral results in an under-prediction.

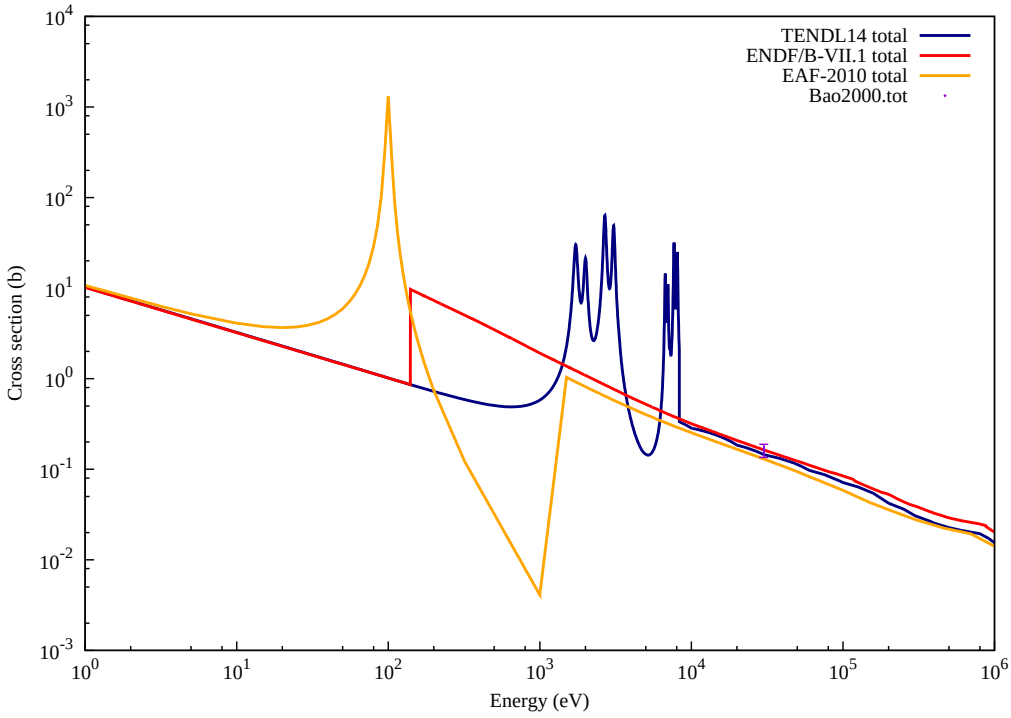

Figure 17: Microscopic ^{65}Zn capture cross sections with EXFOR datapoints. The EAF single resonance approximation is shown, as well as the 100 eV discontinuous model of ENDF/B-VII.1. Note the inclusion of Bao as differential, which is only approximately accurate when the effective Wecott factor is 1.

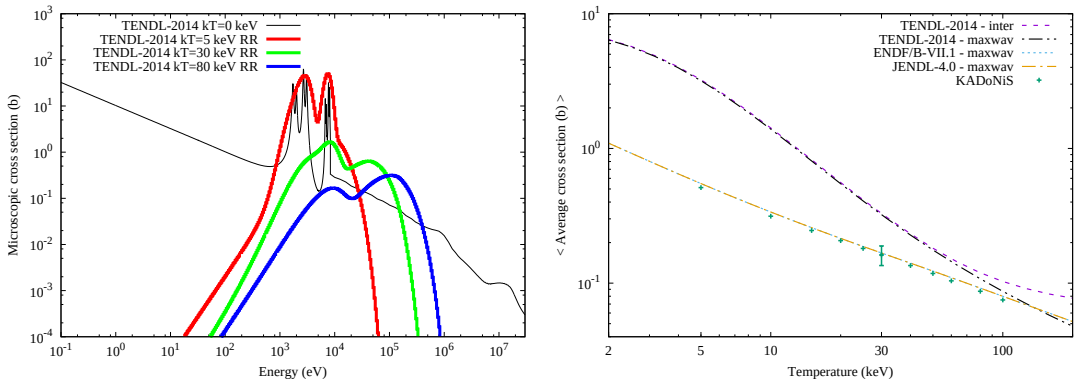

Figure 18: Microscopic kT=0 ^{65}Zn capture cross sections with normalised reaction rates for kT=5, 30 and 80 keV (left). Comparison of average Maxwellian capture cross section over temperature for ^{65}Zn (right). The statistically resolved resonances provide vast majority of the reaction rate, causing disagreement with the experiments.

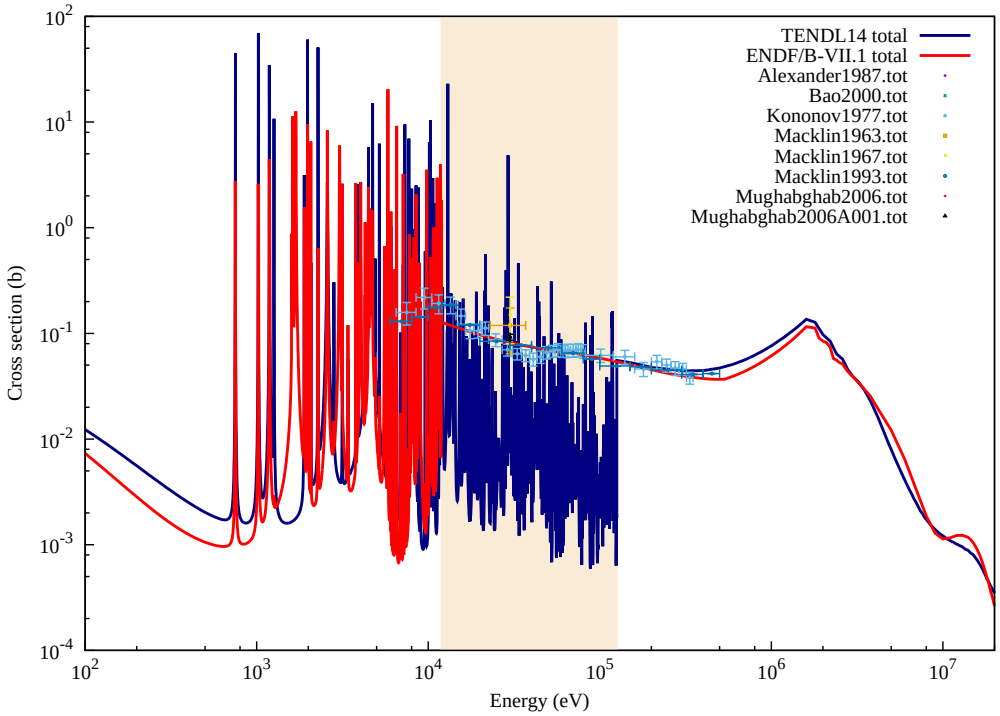

Figure 19: Microscopic ^{144}Sm capture cross sections with EXFOR datapoints. The statistically resolved resonance region is highlighted, which does not reproduce the average values which have been measured.

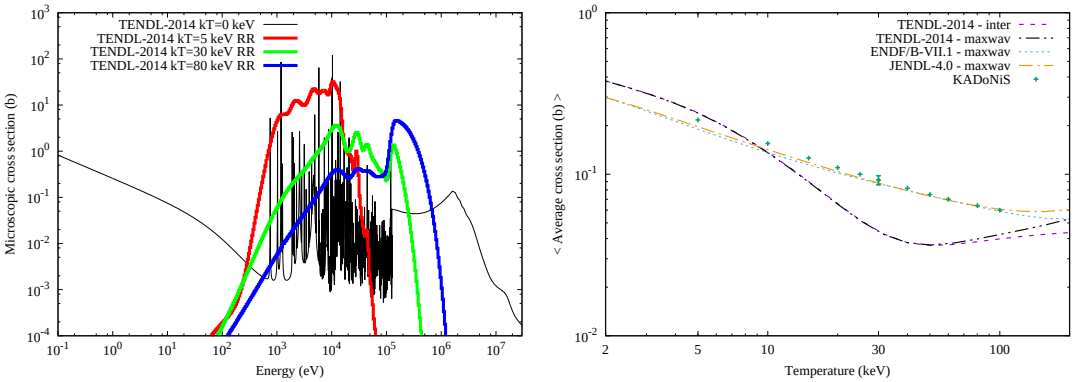

Figure 20: Microscopic kT=0 ^{144}Sm capture cross sections with normalised reaction rates for kT=5, 30 and 80 keV (left). Comparison of average Maxwellian capture cross section over temperature for ^{144}Sm (right). The under-predicted region between 10-100 keV results in significant disagreement with the KADoNiS values.

3 Discussion

While several issues for TENDL-2014 have been brought up in the reports cited and summarised in this report, it should be stressed that the overall performance of the files are impressive in comparison with legacy libraries. The completeness of TENDL offers many advantages but also opens up the library to criticism on a scale that no other evaluators are brave enough to accept.

Fully embracing this approach, future TENDL distributions should be even bolder to provide data for more applications. While the predictions may become less accurate further from well-known regimes (*i.e.* around stability), the additional information will generally not affect more 'standard' systems but give some applications unique data. From experience it is clear that the easily implemented choice of 0.1 second half-life threshold for daughter products is overly restrictive. Several examples of experimental data on shorter-lived isomers are available, for example [16]:

^{23}Na(n,γ)^{24m}Na	^{71}Ga(n,γ)^{72m}Ga
^{87}Rb(n,γ)^{87m}Rb	^{113}In(n,γ)^{114n}In
^{143}Nd(n,α)^{140m}Ce	^{147,149}Sm(n,α)^{144m,146m}Nd
^{153,155,157}Gd(n,α)^{150m,152m,154m}Sm	^{154}Gd(n,γ)^{155m}Gd
^{169}Tm(n,γ)^{170m}Tm	^{179}Hf(n,γ)^{180n}Hf
^{189}Os(n,γ)^{190m}Os	^{253}Es(n,γ)^{254m}Es

In some cases the automatic restrictions come at odds with the (admittedly man-made) standard isomer identification scheme, such as ^{177}Lu which has [7/2+], [1/2+] and [23/2-] states with half-lives of 6.6 days, 0.16 ms and 160 days, respectively. They are commonly referred to as 'g', 'm' and 'n' isomers, while TENDL-2014 omits the second.

Another less known but potentially important, self-imposed TALYS limit is the number of neutrons and protons any reaction is allowed to eject. While for many applications the TENDL-2014 values of `numN=34` and `numZ=14` are more than satisfactory, specific systems will require more general results.

A Appendix

A.1 Discrepant thermal cross sections

Table 1: Summary of TENDL-2014 thermal cross sections with C/E <0.5 or C/E >2.0. Those marked with (M) have been measured in a 0.0253 eV Maxwellian neutron spectrum.

Reaction	σ_E(b)	$\Delta\sigma_E$(b)	σ_{T14}(b)	C/E
Na22(n,a)	2.62E+02	19.1 %	2.62E-01	**0.001**
Al26(n,a)	3.35E-01	4.2 %	3.35E-04	**0.001**
Ar37(n,a)	1.97E+03	16.8 %	1.97E+00	**0.001**
Ni59(n,a)	1.23E+01	4.9 %	1.23E-02	**0.001**
Zn65(n,a)	2.00E+00	10 %	1.99E-03	**0.001**
Zn70(n,g)m	8.70E-03	5.7 %	2.18E-02	2.50
Sr86(n,g)g	2.30E-01	13 %	3.96E-02	0.17
Nb94(n,g)m	6.00E-01	16.7 %	4.96E-02	**0.08**
Pd106(n,g)m	6.86E-03	94.2 %	5.63E-04	**0.08**
Pd108(n,g)m	1.85E-01	5.4 %	6.00E-02	0.32
Pd110(n,g)m	3.30E-02	9.1 %	1.08E-03	**0.03**
Cd109(n,a)	5.00E-02	-	4.96E-05	**0.001**
Cd110(n,g)m	1.07E-01	67.9 %	2.49E-01	2.33
Cd113(n,a)	3.90E+00	10.3 %	9.99E-07	**2.5E-07**
Cd116(n,g)m	1.56E-02	64.1 %	7.14E-03	0.46
In115(n,g)g	4.00E+01	5 %	5.05E-20	**1.3E-21**
In115(n,g)m	8.10E+01	9.9 %	7.80E+02	9.63
In115(n,g)n	8.10E+01	9.9 %	3.09E+01	0.38
Sn116(n,g)m	3.50E-03	14.3 %	1.13E-03	0.32
Te120(n,g)m	3.40E-01	17.6 %	1.44E-01	0.42
Sb121(n,g)m	6.00E-02	16.7 %	1.02E-02	0.17
Sn122(n,g)g	4.10E-03	29.3 %	3.72E-02	9.07
Sb123(n,g)m	4.53E-01	91.8 %	9.16E-01	2.02
Te124(n,g)m	8.51E-01	7.2 %	4.24E-01	0.50
Te126(n,g)m (M)	5.60E-02	5.4 %	1.85E-02	0.33
Te128(n,g)m	2.00E-02	10 %	3.68E-03	0.18
Xe126(n,g)m	4.80E-01	20.8 %	2.20E-01	0.46
Xe128(n,g)m	1.93E-01	148.7 %	7.97E-02	0.41
Xe132(n,g)m	2.63E-02	90.5 %	2.94E-03	0.11
Cs133(n,g)m	2.70E+00	4.8 %	1.98E-01	**0.07**
Ba130(n,g)m	9.80E-01	5.1 %	2.47E-01	0.25
Ba132(n,g)m	5.00E-01	-	1.46E-01	0.29
Ba134(n,g)m	1.34E-01	17.9 %	5.29E-02	0.39
Ce136(n,g)m	9.50E-01	26.3 %	7.27E-02	**0.08**
Eu152m(n,g)	1.84E+04	21.7 %	7.13E+04	3.88
Gd153(n,a)	2.10E-02	-	3.69E-03	0.18

Reaction	σ_E(b)	$\Delta\sigma_E$(b)	σ_{T14}(b)	C/E
Gd155(n,a)	8.20E-05	13.4 %	1.48E-05	0.18
Hf178n(n,g)	4.40E+02	-	1.90E+03	4.32
Ta181(n,g)n	6.84E-03	90.1 %	9.78E-04	0.14
Ta181(n,g)m	3.59E+00	-	7.43E+00	2.07
Os190(n,g)g	3.90E+00	2.6 %	1.39E+00	0.36
Ir191(n,g)n	3.10E-02	45.2 %	1.56E-03	**0.05**
Pt192(n,g)m	2.20E+00	36.4 %	9.57E-02	**0.04**
Pt194(n,g)m	3.60E-02	11.1 %	3.52E-03	**0.1**
Pt196(n,g)m	4.40E-02	9.1 %	8.47E-03	0.19
Pt198(n,g)m	3.50E-01	11.4 %	7.73E-05	**2.2E-04**
Au197(n,g)m	8.00E-03	25 %	4.71E-04	**0.06**
Hg196(n,g)m	1.07E+02	1.4 %	6.58E+00	**0.06**
Hg198(n,g)m	1.80E-02	22.2 %	2.80E-03	0.16
Hg200(n,g) (M)	6.00E+01	-	2.99E+01	0.50
Bi209(n,g)m	1.77E-02	4 %	6.39E-03	0.36
Pa225(n,f)	3.37E+01	-	1.62E+01	0.48
Pa227(n,f)	4.90E-01	-	4.35E+00	8.88
Pa230(n,f)	1.50E+03	16.7 %	4.66E+02	0.31
Pa233(n,g)m	2.01E+01	15.9 %	7.83E+00	0.39
Th232(n,f)	5.20E-05	76.9 %	7.15E-04	**13.75**
Np239(n,g)m	3.20E+01	18.8 %	1.60E+01	0.50
Pu234(n,f)	3.97E+02	-	1.27E+02	0.32
Pu244(n,f)	2.80E-03	-	1.71E-02	6.11
Am237(n,f)	2.55E+02	-	6.79E+01	0.27
Am243(n,g)m	5.50E+01	-	2.38E+01	0.43
Am243(n,g)g	2.01E+01	81.1 %	5.13E+01	2.55
Cm240(n,f)	2.15E+03	-	8.76E+02	0.41
Bk243(n,f)	6.78E+02	-	1.74E+02	0.26
Es254m(n,g)	1.83E+03	4.4 %	7.82E+02	0.43
Es254(n,g) (M)	2.83E+01	8.8 %	9.84E+01	3.48
Fm254(n,f)	2.88E+03	-	2.02E+02	**0.07**
Fm255(n,f)	3.36E+03	5.1 %	1.66E+03	0.49
Fm257(n,f)	2.95E+03	5.4 %	7.46E+02	0.25

A.2 Discrepant resonance integral cross sections

Table 2: Summary of TENDL-2014 integral resonance cross sections with C/E <0.5 or C/E >2.0.

Reaction	σ_E(b)	$\Delta\sigma_E$(b)	σ_{T14}(b)	C/E
N15(n,g)	1.10E-04	27.3 %	3.21E-05	0.29
Na22(n,p)	1.37E+05	8.8 %	1.25E+04	**0.09**
Na22(n,abs)	2.00E+05	25 %	3.12E+04	0.16
Si30(n,g)	6.30E-01	4.8 %	7.11E-02	0.11
Cl35(n,p)	6.00E-01	-	2.26E-01	0.38
Cl36(n,p)	4.20E-02	-	7.04E-01	**16.76**
Sc45(n,g)m	5.40E+00	11.1 %	2.66E+00	0.49
Co58m(n,g)	1.40E+05	7.1 %	4.06E+04	0.29
Ni65(n,g)	1.00E+01	10 %	1.65E+02	**16.55**
Ge73(n,g)	6.30E+02	1.1 %	6.43E+01	**0.10**
Ge74(n,g)m	4.10E-01	17.1 %	1.38E-01	0.34
Se80(n,g)m	1.47E-01	3.4 %	3.12E-01	2.12
Sr84(n,g)g	7.40E-01	27 %	2.42E+00	3.27
Kr86(n,g)	1.00E-03	-	1.35E-02	**13.49**
Sr88(n,g)	6.50E-02	46.2 %	2.37E-02	0.37
Rb88(n,g)	5.00E-01	20 %	1.30E+00	2.61
Ru103(n,g)	5.00E+00	-	4.73E+01	9.47
Rh103(n,g)m	7.50E+01	6.7 %	3.41E+01	0.45
Pd106(n,g)m	2.00E-01	-	2.54E-02	0.13
Pd110(n,g)m	6.60E-01	10.6 %	8.99E-03	**0.01**
Cd110(n,g)m	3.90E+00	2.6 %	9.24E-01	0.24
Ag110m(n,g)	2.00E+01	20 %	8.21E+01	4.11
In115(n,g)g	6.50E+02	4.6 %	2.85E+01	**0.04**
In115(n,g)m	2.65E+03	3.8 %	1.23E+04	4.64
In115(n,g)n	1.50E+03	-	4.93E+02	0.33
Sn116(n,g)m	4.90E-01	32.7 %	1.14E-01	0.23
Te120(n,g)	1.00E+00	-	7.25E+00	7.25
Te122(n,g)	2.80E+01	35.7 %	8.92E+01	3.19
Te127(n,g)	1.14E+03	14.9 %	1.99E+02	0.17
Te128(n,g)m	7.75E-02	6.5 %	2.50E-02	0.32
Sb121(n,g)m	1.30E+01	7.7 %	3.74E-01	**0.03**
Sn124(n,g)g	8.30E-02	30.1 %	3.56E-01	4.29
Ba130(n,g)g	2.30E+01	4.3 %	1.69E+02	7.34
Ba130(n,g)m	1.53E+02	4.6 %	5.00E+00	**0.03**
Ba132(n,g)m	2.80E+00	-	1.30E+00	0.46
Ba134(n,g)m	2.39E+01	15.9 %	7.82E-01	**0.03**
Ba135(n,g)m	4.65E-01	15.1 %	1.78E-01	0.38
Ba136(n,g)m	1.00E-01	-	4.89E-02	0.49
Ba139(n,g)	2.20E+00	22.7 %	8.96E+00	4.07

Reaction	σ_E(b)	$\Delta\sigma_E$(b)	σ_{T14}(b)	C/E
I131(n,g)	8.00E+00	5 %	9.60E+01	**12.00**
Xe132(n,g)m	9.00E-01	22.2 %	3.39E-02	**0.04**
Cs133(n,g)m	2.90E+01	3.8 %	2.69E+00	**0.09**
Ce138(n,g)m	1.50E+00	-	1.19E-01	**0.08**
Nd142(n,g)	3.40E+01	32.4 %	6.13E+00	0.18
Sm145(n,g)	6.00E+02	15 %	2.89E+03	4.81
Eu152m(n,g)	1.00E+05	-	4.57E+04	0.46
Eu154(n,g)	8.02E+02	24.9 %	1.88E+03	2.35
Ho166m(n,g)	1.00E+04	27 %	1.18E+03	0.12
Yb169(n,g)	5.20E+03	9.6 %	2.45E+03	0.47
Tm170(n,g)	4.60E+02	10.9 %	1.66E+03	3.60
Tm171(n,g)	4.60E+02	10.9 %	9.73E+02	2.12
Er171(n,g)	1.70E+02	11.8 %	1.42E+03	8.35
Lu177m(n,g)	1.40E+00	14.3 %	1.43E+01	**10.20**
Hf178(n,g)g	8.50E+02	-	3.89E+02	0.46
Ta180(n,g)	1.35E+03	7.4 %	6.70E+03	4.96
Ta181(n,g)n	4.15E-01	26.5 %	3.24E-02	**0.08**
W180(n,g)	2.14E+02	14 %	6.36E+02	2.97
Os186(n,g)	2.54E+02	11.8 %	8.06E+00	**0.03**
Os191(n,g)	1.70E+02	17.6 %	5.84E+02	3.43
Pt192(n,g)	1.18E+02	25.4 %	1.87E+01	0.16
Pt194(n,g)m	1.00E+00	10 %	2.37E-02	**0.02**
Pt196(n,g)m	3.50E-01	20 %	9.78E-02	0.28
Pt198(n,g)m	6.00E+00	11.7 %	1.37E-03	**2.3E-04**
Pt199(n,g)	7.00E+00	-	4.64E+01	6.63
Au197(n,g)m	6.00E-02	33.3 %	7.55E-03	0.13
Hg196(n,g)m	5.89E+01	4.1 %	9.54E-01	**0.02**
Hg198(n,g)m	1.80E+00	16.7 %	9.18E-02	**0.05**
Hg200(n,g)	1.50E+00	33.3 %	4.28E+01	**28.53**
Pb205(n,g)	2.00E+00	-	7.90E+00	3.95
Pb206(n,g)	2.23E-01	62.8 %	9.12E-02	0.41
Ac227(n,g)	1.66E+03	4.8 %	4.89E+02	0.29
Th231(n,f)	1.56E+02	-	4.99E+02	3.20
Th232(n,f)	7.46E-02	2.1 %	8.34E-03	0.11
Th233(n,f)	8.40E+01	-	2.12E+02	2.53
Pa233(n,g)m	4.38E+02	16 %	1.75E+02	0.40
U233(n,abs)	8.97E+02	2.2 %	1.41E+02	0.16
U235(n,abs)	4.19E+02	1.9 %	1.40E+02	0.33
Np236m(n,f)	1.35E+03	6.4 %	3.94E+02	0.29
Np237(n,f)	4.70E+00	4.9 %	5.49E-01	0.12
Np238(n,abs)	1.50E+03	33.3 %	2.44E+02	0.16
Pu241(n,abs)	7.32E+02	2.3 %	1.80E+02	0.25
Am241(n,f)	1.44E+01	6.9 %	7.27E+00	0.50
Am242m(n,f)	1.57E+03	5.1 %	3.72E+02	0.24

Reaction	σ_E(b)	$\Delta\sigma_E$(b)	σ_{T14}(b)	C/E
Am242m(n,g)	2.11E+02	-	6.80E+01	0.32
Am242(n,f)	3.00E+02	-	9.91E+02	3.30
Am243(n,f)	8.50E+00	5.9 %	2.48E+00	0.29
Am243(n,g)g	9.40E+01	9.6 %	1.23E+03	**13.08**
Am243(n,g)m	1.73E+03	4 %	5.70E+02	0.33
Cm244(n,f)	1.25E+01	20 %	6.04E+00	0.48
Cm248(n,f)	1.31E+01	11.5 %	2.89E+00	0.22
Cf250(n,f)	1.60E+02	25 %	7.68E+02	4.80
Cf251(n,f)	5.90E+03	1.7 %	1.31E+03	0.22
Cf253(n,f)	2.00E+03	20 %	2.02E+02	**0.10**
Cf254(n,g)	2.00E+00	-	1.03E+01	5.17
Es253(n,g)m	3.75E+03	5.3 %	7.25E+02	0.19
Es253(n,g)g	1.14E+02	6.1 %	8.54E+02	7.49
Es254m(n,g)	1.00E+03	-	1.48E+02	0.15

A.3 Discrepant Maxwellian-averaged cross sections

Table 3: Comparison of KADoNiS 5, 30 and 80 keV MACS against collapsed nuclear data values. Only 30 keV uncertainties are provided and all statistical model calculations are indicated in red with (SMC).

	KADoNiS	$\Delta\sigma_E$	TENDL-2014			ENDF/B7.1	JENDL4.0
	σ(b)	%	σ(b)	R(cm^3/s)	C/E	C/E	C/E
He3							
30keV	7.60E-06	7.9	2.13E-05	3.56E+03	2.80	2.80	2.16
C14							
5keV	3.62E-06		7.32E-09	4.48E-01	0.00	—	—
30keV	8.48E-06	6.7	1.49E-08	2.23E+00	0.00	—	—
80keV	1.27E-05		7.32E-09	6.36E+00	0.00	—	—
O18							
5keV	3.70E-06		1.70E-05	1.03E+03	4.60	—	—
30keV	8.90E-06	9.0	4.89E-04	7.28E+04	54.92	—	—
80keV	2.23E-05		1.70E-05	8.24E+04	15.20	—	—
Si28							
5keV	1.40E-04		2.66E-04	1.60E+04	1.90	2.99	2.99
30keV	1.42E-03	9.2	5.80E-03	8.56E+05	4.09	2.54	2.54
80keV	1.08E-03		2.66E-04	7.11E+05	2.73	2.19	2.19
S36							
5keV	4.20E-04		3.50E-04	2.10E+04	0.83	3.10	3.10
30keV	1.71E-04	8.2	7.60E-04	1.12E+05	4.45	3.70	3.70
80keV	1.10E-04		3.50E-04	1.31E+05	4.97	3.84	3.84
Ar39 (SMC)							
5keV	3.50E-02		2.17E+00	1.30E+08	61.95	—	—
30keV	8.00E-03	25.0	1.50E+00	2.20E+08	187.60	—	—
80keV	3.80E-03		2.17E+00	9.93E+07	109.08	—	—
Ho163							
5keV	5.81E+00		2.30E+01	1.36E+09	3.95	—	—
30keV	2.12E+00	4.5	5.97E+00	8.68E+08	2.81	—	—
80keV	1.37E+00		2.30E+01	7.36E+08	2.26	—	—
Hg200							
5keV	3.24E-01		5.43E+00	3.22E+08	16.76	0.82	0.82
30keV	1.15E-01	10.4	1.19E+00	1.73E+08	10.34	1.11	1.11
80keV	8.60E-02		5.43E+00	8.97E+07	4.40	0.98	0.98
Hg203 (SMC)							
5keV	3.75E-01		1.71E+00	1.01E+08	4.55	—	—
30keV	9.80E-02	17.3	3.86E-01	5.61E+07	3.94	—	—
80keV	4.90E-02		1.71E+00	5.00E+07	4.30	—	—

A.4 Other integral cross sections

The following comparisons are due almost entirely to measurements taken from neutron sources with deuteron beams into tritiated targets, with one from a lithium target. These values are taken from CCFE-R(15)27 [2] with additional detailed analysis from CCFE-R(15)25 [1].

Table 4: Summary of TENDL-2014 C/E values for several discrepant integral measurements supported by differential measurements.

Reaction	Experiment	σ_E(b)	$\Delta\sigma_E$(b)	C/E
Rh-103(n,g)Rh-104	fns_5min	2.66E-02	2.12E-03	2.50
In-115(n,g)In-116	fns_5min	5.67E-02	2.83E-03	11.11
Sn-118(n,2n)Sn-117m	fns_7hour	9.50E-01	1.14E-01	0.80
	fng_Sn	1.32E+00	3.27E-02	0.57
I-127(n,g)I-128	fns_5min	1.93E-02	1.16E-03	1.72
Nd-150(n,2n)Nd-149	fns_5min	8.29E-01	1.24E-01	1.72
Tb-159(n,p)Gd-159	fns_5min	2.04E-02	3.93E-02	0.25
Dy-164(n,g)Dy-165g	fng_Dy	2.97E-02	1.34E-03	0.58
Dy-164(n,g)Dy-165m	fns_5min	1.01E-01	1.51E-02	1.30
Dy-164(n,g)Dy-165	fns_5min	3.56E-02	8.19E-03	5.26
Ho-165(n,2n)Ho-164m	fns_5min	7.14E-01	1.00E-01	1.19
Hf-179(n,p)Lu-179	fng_hafnium	1.08E-02	2.51E-03	0.28
Hf-180(n,n')Hf-180m	fng_hafnium	1.14E-02	6.65E-04	2.53
	fns_5min	1.80E-02	1.44E-03	1.64
Hf-180(n,g)Hf-181	fng_hafnium	9.28E-03	1.51E-03	0.40
Hf-180(n,p)Lu-180	fns_5min	3.52E-03	2.11E-04	0.68
	fng_hafnium	3.87E-03	9.36E-04	0.62
	fng_heat	6.88E-03	5.44E-04	0.36
Ta-181(n,g)Ta-182	fng_Ta	4.21E-02	2.90E-03	0.69
	fns_7hour	1.09E-02	2.41E-03	0.43
Ta-181(n,g)Ta-182n	fng_Ta	1.20E-04	4.13E-05	0.30
Ta-181(n,a)Lu-178g	fng_Ta	1.01E-03	4.04E-04	0.42
W-182(n,a)Hf-179n	rez_DF	1.85E-05	1.81E-06	12.29
W-186(n,2n)W-185m	fns_5min	3.22E-01	4.18E-02	2.00
Hg-200(n,2n)Hg-199m	fns_5min	7.87E-01	6.30E-02	1.18
Pb-206(n,a)Hg-203	tud_Pb	5.02E-04	5.42E-05	0.96
	fns_7hour	1.57E-03	1.00E-03	0.33
Pb-208(n,p)Tl-208	fns_5min	9.98E-04	5.99E-05	0.72
	tud_Pb	8.38E-04	8.88E-05	0.71

B FNS decay heat discrepancies

The discrepancies found in the FNS fusion decay heat validation report [1] are summarised below with the same figures which appeared in that report. Four simulations are performed for each irradiation and compared with the results from FNS. Nuclides are listed at the (x,y) position which represents their ($t_{1/2}$,heat(t=EOI)). As such, they identify the dominant nuclides at the various cooling times.

Take as an example the rhodium irradiation simulations of Figure 21, which shows four decay heat curves from TENDL-2014, JEFF-3.2, JENDL-4.0 and ENDF/B-VII.1. Only the first two contain the ^{103}Rh(n,n')^{103m}Rh channel, although both appear to over-predict ^{103m}Rh production when compared with the FNS results. When analysed against the differential cross sections, these provide a powerful tool for validation and error-spotting.

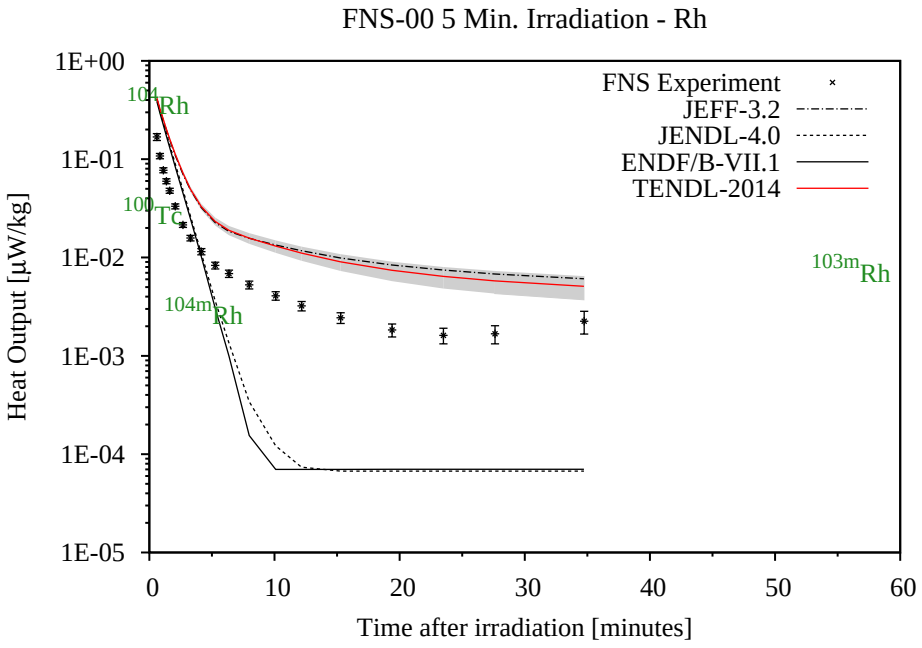

Figure 21: FNS decay heat measurements from 5 minute irradiation of rhodium. While other libraries miss the ^{103}Rh(n,n')^{103m}Rh channel, this experiment suggests that it is over-predicted in TENDL-2014.

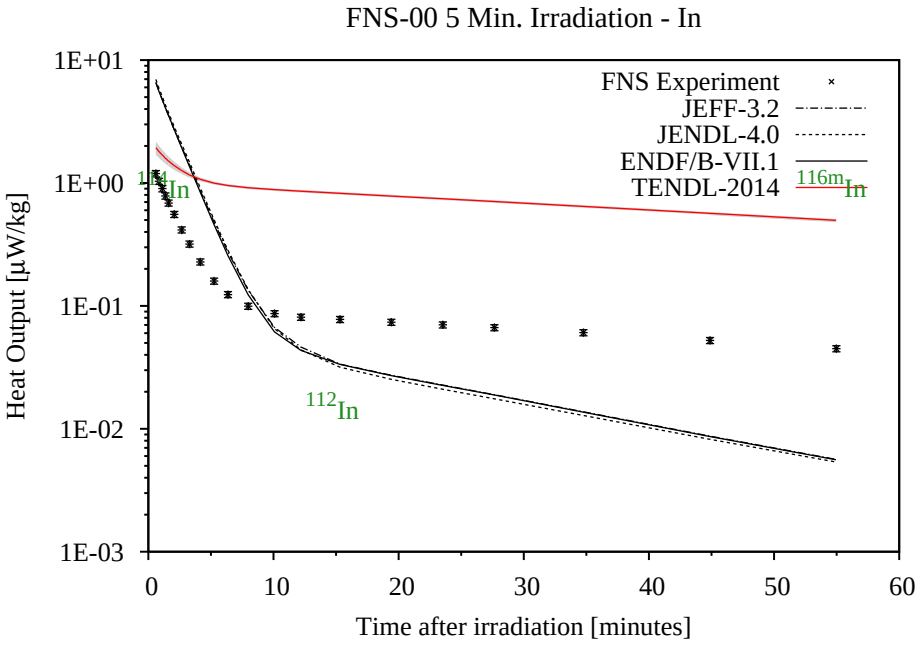

Figure 22: FNS decay heat measurements from 5 minute irradiation of indium. An error in the `MF=9` branching results in a grossly over-estimated ^{116m}In capture product.

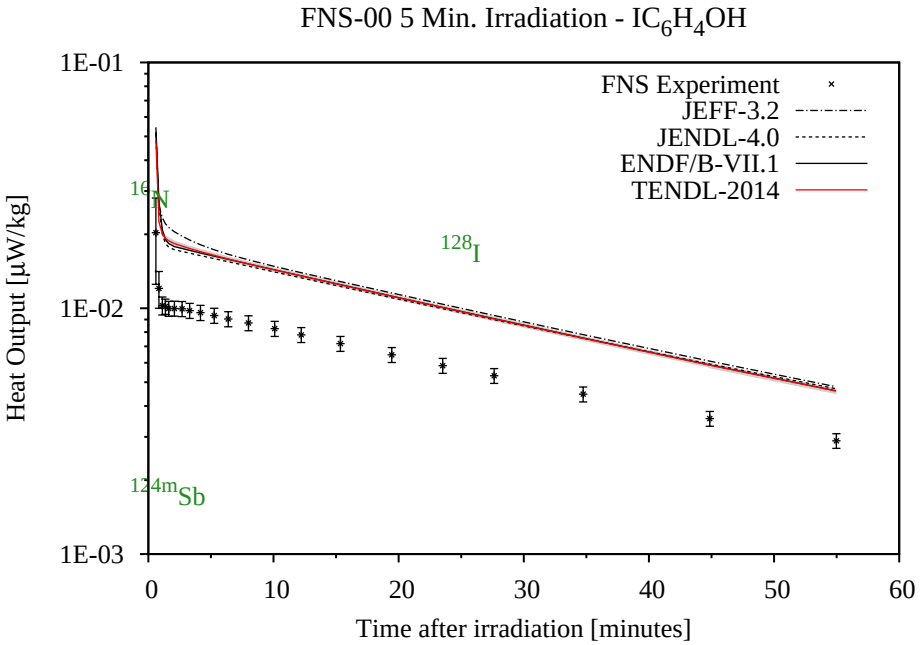

Figure 23: FNS decay heat measurements from 5 minute irradiation of iodine. The ^{127}I(n,γ) is over-predicted by TENDL-2014 in the FNS neutron spectrum.

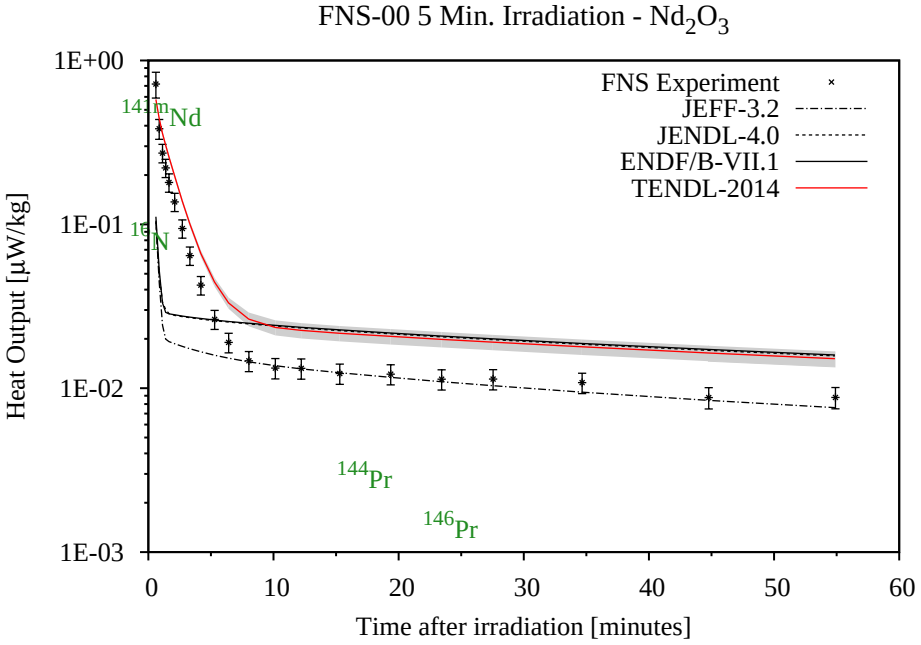

Figure 24: FNS decay heat measurements from 5 minute irradiation of neodymium. ^{149}Nd, mostly produced through ^{150}Nd(n,2n), is over-predicted.

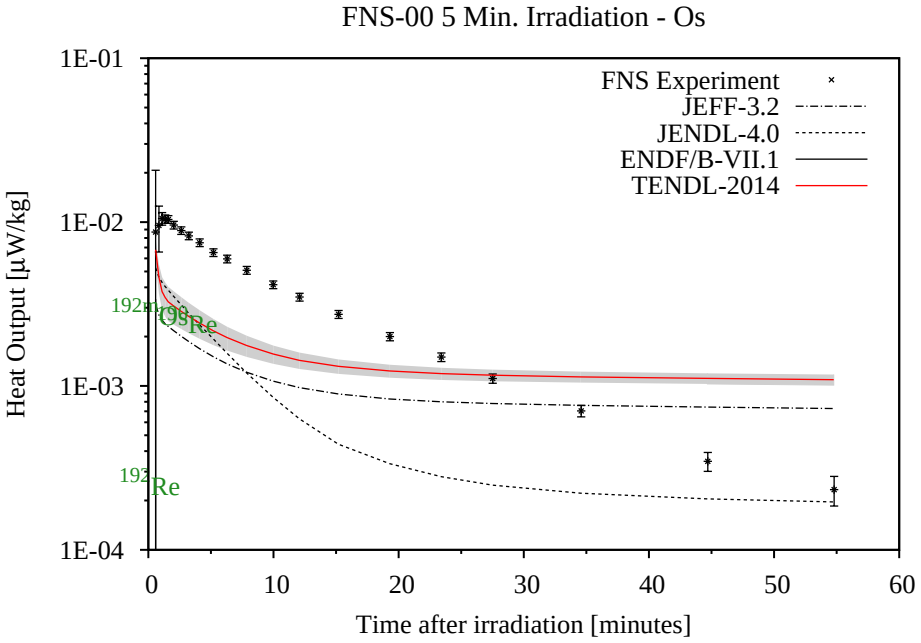

Figure 25: FNS decay heat measurements from 5 minute irradiation of osmium. This presents a non-trivial problem with mixing of isomeric branching ratios from multiple reactions, including inelastic, capture and (n,2n) on various Os isotopes.

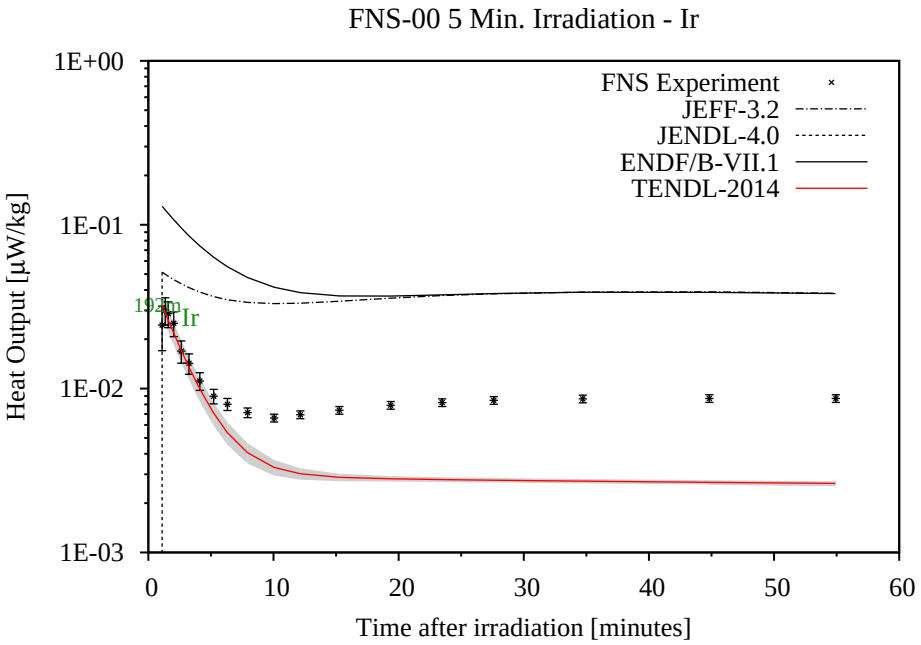

Figure 26: FNS decay heat measurements from 5 minute irradiation of iridium. Other libraries appear to grossly over-predict ^{190}Re production, as well as ^{190m}Os, through the inelastic channel not open in TENDL-2014.

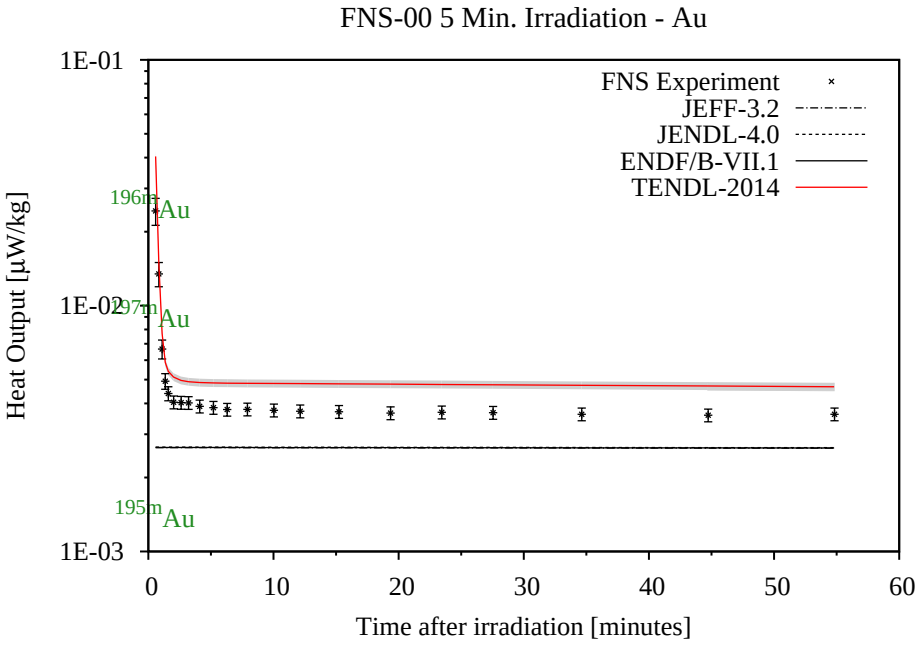

Figure 27: FNS decay heat measurements from 5 minute irradiation of gold. TENDL-2014 is the only library containing the necessary isomeric production cross sections. The discrepancy with FNS is due to some ^{197}Au(n,2n)^{196g,n}Au under-predictions.

References

[1] J.-Ch. Sublet and M. Gilbert, "Decay heat validation, FISPACT-II & TENDL-2014, JEFF-3.2, ENDF/B-VII.1 and JENDL-4.0 nuclear data libraries," Tech. Rep. CCFE-R(15)25, CCFE, 2015. http://www.ccfe.ac.uk/FISPACT.aspx.

[2] M. Fleming, J.-Ch. Sublet, and J. Kopecky, "Integro-Differential Verification and Validation, FISPACT-II & TENDL-2014 nuclear data libraries," Tech. Rep. CCFE-R(15)27, CCFE, March 2015. http://www.ccfe.ac.uk/FISPACT.aspx.

[3] J.-Ch. Sublet and M. Fleming, "Maxwellian-Averaged Neutron-Induced Cross Sections for kT=1 keV to 100 keV, KADoNiS, TENDL-2014, ENDF/B-VII.1 and JENDL-4.0u nuclear data libraries," Tech. Rep. UKAEA-R(15)29, UKAEA, March 2015. http://www.ccfe.ac.uk/FISPACT.aspx.

[4] M. Fleming, J.-Ch. Sublet, J. Kopecky, D. A. Rochman, and A. J. Koning, "Probing experimental & systematic trends of the neutron-induced TENDL-2014 nuclear data library," Tech. Rep. UKAEA-R(15)30, UKAEA, October 2015. http://www.ccfe.ac.uk/FISPACT.aspx.

[5] H. Liu, M. A. Abdou, and L. R. Greenwood, "^{55}Fe effect on enhancing ferritic steel He/dpa ratio in fission reactor irradiations to simulate fusion conditions ," *Fusion Engineering and Design*, vol. 88, no. 11, pp. 2860 – 2864, 2013.

[6] T. Gaines. Private communication, September 2015. AWE.

[7] F. Maekawa and Y. Ikeda, "Decay heat experiment on thirty-two fusion reactor relevant materials irradiated by 14-MeV neutrons," *Fusion Engineering and Design*, vol. 47, no. 4, pp. 377 – 388, 2000.

[8] F. Maekawa, K.-i. Shibata, Y. Ikeda, H. Takeuchi, and M. Wada, *Comprehensive activation experiment with 14-MeV neutrons covering most of naturally existing elements 5 minutes irradiation experiment.* Japan: Atomic Energy Society of Japan, 2002.

[9] M. Pillon, "Decay heat in tantalum irradiated in a first-wall like neutron spectrum. measurement and analyses," Tech. Rep. FUS-TN-MA-NE-R-11, ENEA, 2005.

[10] E. M. Zsolnay, R. N. Capote, H. J. Nolthenius, and A. Trkov, "Summary Description of the New International Reactor Dosimetry and Fusion File (IRDFF release 1.0)," Tech. Rep. INDC(NDS)-0616, IAEA, 2012. https://www-nds.iaea.org/IRDFF/.

[11] A. Koning, S. Hilaire, and S. Goriely, "TALYS-1.7, User Manual," *Nuclear Research and Consultancy Group NRG, Petten*, 2015.

[12] M. Pillon, "Measurements of nuclear decay heat and gamma activation in hafnium samples," Tech. Rep. EFF–DOC-794, 2001.

[13] M. Pillon, M. Angelone, and R. A. Forrest, "Measurements of decay heat and validation of the european activation code system for fusion power plant applications," *Fusion Engineering and Design*, vol. 63-64, no. 0, pp. 101 – 106, 2002.

[14] Y. Kasugi, H. Yamamoto, K. Kawade, Y. Ikeda, Y. Uno, and H. Maekawa, "Activation Cross Section Measurement of Reactions Producing Short-Lived Nuclei at Neutron Energy Between 13.4 MeV and 14.9 MeV," (Gatlinburg), p. 935, JAEA, Nuclear Data for Science and Technology, 1994.

[15] S. Murahira, Y. Satoh, N. Honda, A. Takahashi, T. Iida, M. Shibata, H. Yamamoto, and K. Kawade, "Measurement of Formation Cross Sections Producing Short-Lived Nuclei by 14 MeV Neutrons - Pr, Ba, Ce, Sm, W, Sn, Hf," Tech. Rep. JAERI-CONF–96-008, JAERI, November 1995.

[16] S. F. Mughabghab, *Atlas of Neutron Resonances: Resonance Parameters and Thermal Cross Sections. Z=1-100*. Elsevier, 5 ed., April 2006.